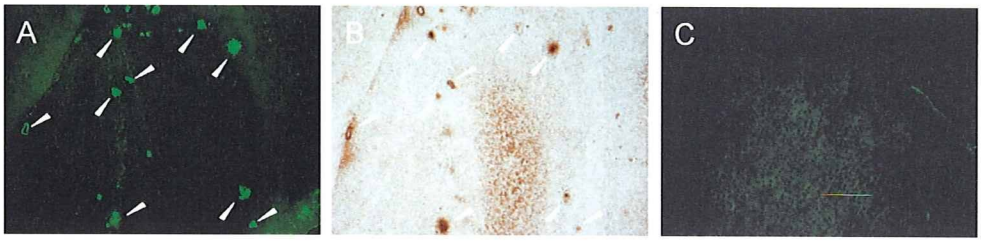

Figure 1. Neuropathological staining of 10 μm sections of a Tg2576 mouse brain (A and B) and aged normal brain (C). Fluorescent staining of compound **7c** in the Tg2576 mouse brain (A). Aβ immunostaining with antibody BC05 in the adjacent section (B). Fluorescent staining of compound **7c** in the age-matched control mouse brain (C).

derivatives was in the same range as that of the known compound, 6-iodo-2-(4′-dimethylamino)phenyl-imidazo[1,2-*a*]pyridine (IMPY), which is commonly used for inhibition assays.[22−25] We selected the dimethylamino derivatives (**7a**, **7b**, **7c**, and **13**), which showed the greatest affinity, for additional studies.

To evaluate brain uptake of the FPEG chalcones, biodistribution experiments were performed in normal mice with four ^{11}C-labeled FPEG chalcones ([^{11}C]**7a**, [^{11}C]**7b**, [^{11}C]**7c**, and [^{11}C]**13**) (Table 2). Because normal mice were used for the biodistribution experiments, no Aβ plaques were expected in the young mice; therefore the washout of probes from the brain should be rapid to obtain a higher signal-to-noise ratio earlier in the AD brain. Radioactivity after injection of the ^{11}C-labeled FPEG chalcones penetrated the blood−brain barrier, showing excellent uptake ranging from 3.7 to 6.0% ID/g brain at 2 min postinjection, a level sufficient for imaging Aβ plaques in the brain. In addition, they displayed good clearance from the normal brain with 2.3, 1.0, 0.35, and 1.0% ID/g at 60 min postinjection for [^{11}C]**7a**, [^{11}C]**7b**, [^{11}C]**7c**, and [^{11}C]**13**, respectively. These values were equal to 37.6, 21.1, 8.1, and 28.3% of the initial uptake peak for [^{11}C]**7a**, [^{11}C]**7b**, [^{11}C]**7c**, and [^{11}C]**13**, respectively. Compound **7c** with the fastest washout from the brain was labeled with ^{18}F and evaluated for its biodistribution in normal mice (Table 3). [^{18}F]**7c** displayed high uptake (3.48%ID/g) at 2 min postinjection, a level sufficient for imaging like [^{11}C]**7c**, and was cleared over the subsequent 10, 30, and 60 min. The radioactivity in the brain at 60 min postinjection was 1.07%ID/g, indicating that this [^{18}F]**7c** has favorable pharmacokinetics in the brain. Although we consider that a slight difference of the radioactivity pharmacokinetics between [^{11}C]**7c** and [^{18}F]**7c** could be attributable to the different physicochemical characteristics of their radiometabolites produced in the brain, the reason for this difference has remained unclear. Bone uptake at 60 min was measurable (3.58%ID/g), suggesting defluorination in vivo. Bone uptake has been observed for other ^{18}F tracers.[12,22−24] However, previous reports suggested that free fluoride was not taken up by brain tissue; therefore, the interference from free fluoride may be relatively low for brain imaging. A previous paper regarding the most promising ^{18}F-labeled agent **4** reported that it showed high uptake (7.77% ID/g at 2 min postinjection) and rapid clearance from the brain (1.61%ID/g at 60 min postinjection) with little accumulation in bone (1.77%ID/g at 60 min postinjection) in biodistribution experiments using normal mice.[12] The pharmacokinetics of **4** appear superior to that of [^{18}F]**7c**, but the good biological results obtained with [^{18}F]**7c** suggest that further investigation is warranted.

To investigate the ability of the fluorinated chalcones to bind to Aβ plaques in the AD model, fluorescent staining of sections of mouse brain were carried out with compound **7c** (Figure 1). We used Tg2576 transgenic mice as an animal model of Aβ plaque deposition, which express human APP695 with the K670N, M671L Swedish double mutation.[26] By 11−13 months of age, Tg2576 mice show prominent Aβ deposition in the cingulated cortex, entorhinal cortex, dentate gyrus, and CA1 hippocampal subfield and have been frequently used for the evaluation of specific binding of Aβ plaques in in vitro and in vivo experiments.[12,24,27−31] Many Aβ plaques were clearly stained with **7c**, as reflected by the affinity for the aggregates of synthetic Aβ(1−42) in in vitro competition assays (Figure 1A). The labeling pattern was consistent with that observed after immunohistochemical labeling by BC05, a specific antibody for Aβ (Figure 1B), while wild-type mouse brain displayed no significant accumulation of **7c** (Figure 1C). The results indicated that **7c** binds specifically to Aβ plaques in Tg2576 mice brain. A previous report suggested the configuration/folding of Aβ plaques in Tg2576 mice to be different from the tertiary/quaternary structure of Aβ plaques in AD brains.[30,32] In addition, the studies reported with **1** further indicate that the binding of **1** reflects the amount of Aβ plaques in human AD brain but not in Tg2576 mouse brain, and the detectability of Aβ plaques by **1** is dependent on the accumulation of specific Aβ subtypes.[28,29] Therefore, we considered that it should be essential to evaluate the binding affinity for Aβ plaques in human AD brains because our goal is to develop clinically useful probes for in vivo imaging of Aβ plaques in humans.

Next, we investigated the binding affinity of [^{18}F]**7c** for Aβ plaques by in vitro autoradiography in a human AD brain section (Figure 2A). The autoradiographic image of [^{18}F]**7c** showed high levels of radioactivity in some specific areas of the brain section. Furthermore, we confirmed that the hot spots of [^{18}F]**7c** in an AD brain section corresponded with those of in vitro thioflavin-S staining in the same brain section (Figure 2B). In contrast, no significant accumulation of [^{18}F]**7c** was observed in the region without Aβ plaques (Figure 2C). The results demonstrate the feasibility of using [^{18}F]**7c** as a probe for detecting Aβ plaques in the brain of AD patients with PET.

In conclusion, we reported novel FPEG chalcone derivatives, containing an end-capped fluoropolyethylene glycol as in vivo PET imaging agents for Aβ plaques in the brain. The FPEG chalcones with a dimethylamino group displayed greater affinity for synthetic Aβ aggregates than did the monomethylamino and primary amino derivatives. In biodistribution experiments using normal mice, ^{11}C-labeled FPEG chalcones displayed sufficient uptake for the imaging of Aβ plaques in the brain. [^{11}C]**7c** showed the fastest clearance from the brain, probably related to a low nonspecific binding. [^{18}F]**7c** also displayed high uptake in and good clearance from

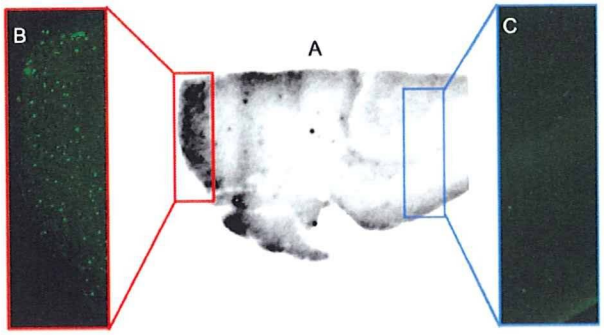

Figure 2. In vitro autoradiography of [^{18}F]**7c** using the human AD brain section (A). Aβ plaques were confirmed by in vitro staining of the same section with thioflavin-S (B and C).

the brain, although a slight difference was observed between the ^{11}C and ^{18}F tracers. When the labeling of plaques in vitro was carried out using sections of brain tissue from an animal model of AD and an AD patient, compound **7c** intensely labeled Aβ plaques existing in both brains. Taken together, the results suggest the novel FPEG chalcone **7c** to be potentially useful for imaging Aβ plaques in the brain using PET.

Experimental Section

General. All reagents were obtained commercially and used without further purification unless otherwise indicated. ^{1}H NMR spectra were obtained on a Varian Gemini 300 spectrometer with TMS as an internal standard. Coupling constants are reported in hertz. Multiplicity was defined by s (singlet), d (doublet), t (triplet) and m (multiplet). Mass spectra were obtained on a JEOL IMS-DX instrument. HPLC analysis was performed on a Shimadzu HPLC system (a LC-10AT pump with a SPD-10A UV detector, $\lambda = 254$ nm) using a Cosmosil C_{18} column (Nakalai Tesque, 5C_{18}-AR-II, 4.6 mm × 150 mm) using acetonitrile/water (50/50) as mobile phase at a flow rate of 1.0 mL/min. All key compounds were proven by this method to show ≥95% purity.

Chemistry. (*E*)-3-(4-(Dimethylamino)phenyl)-1-(4-hydroxyphenyl)-2-propen-1-one (5). 4-Hydroxyacetophenone (1.36 g, 10 mmol) and 4-dimethylaminobenzaldehyde (1.86 g, 10.0 mmol were dissolved in EtOH (15 mL). A 30 mL aliquot of a 10% aqueous KOH solution was then slowly added dropwise to the reaction mixture. The mixture was stirred for 24 h at 100 °C and then extracted with ethyl acetate. After the organic layers were combined and dried over Na_2SO_4, evaporation of the solvent afforded 1.50 g of **5** (84.0%). ^{1}H NMR (CD_3OD) δ: 3.04 (s, 6H), 6.76 (d, $J = 8.7$ Hz, 2H), 6.88 (d, $J = 8.7$ Hz, 2H), 7.50 (d, $J = 15.3$ Hz, 1H), 7.59 (d, $J = 9.0$ Hz, 2H), 7.72 (d, $J = 15.3$ Hz, 1H), 7.98 (d, $J = 8.7$ Hz, 2H). ^{1}H NMR (DMSO-d_6) δ: 2.99 (s, 6H), 6.74 (d, $J = 8.7$ Hz, 2H), 6.88 (d, $J = 8.4$ Hz, 2H), 7.62 (s, 2H), 7.68 (d, $J = 8.7$ Hz, 2H), 8.03 (d, $J = 8.7$ Hz, 2H), 10.30 (s, 1H). EI-MS: m/z 267 (M^+).

(*E*)-3-(4-(Dimethylamino)phenyl)-1-(4-(2-hydroxyethoxy)phenyl)-2-propen-1-one (6a). To a solution of **5** (500 mg, 1.87 mmol and ethylene chlorohydrin (125 μL, 1.87 mmol) in DMSO (5 mL) was added anhydrous K_2CO_3 (775 mg, 5.61 mmol). The reaction mixture was stirred for 18 h at 100 °C and then poured into water and extracted with chloroform. The organic layers were combined and dried over Na_2SO_4. Evaporation of the solvent afforded a residue, which was purified by silica gel chromatography (hexane: ethyl acetate = 1:1) to give 422 mg of **6a** (72.7%). ^{1}H NMR ($CDCl_3$) δ: 3.04 (s, 6H), 4.00−4.01 (m, 2H), 4.17 (t, $J = 4.8$ Hz, 2H), 6.69 (d, $J = 9.0$ Hz, 2H), 6.99 (d, $J = 6.9$ Hz, 2H), 7.35 (d, $J = 15.3$ Hz, 1H), 7.55 (d, $J = 9.0$ Hz, 2H), 7.79 (d, $J = 15.3$ Hz, 1H), 8.02 (d, $J = 9.3$ Hz, 2H).

(*E*)-3-(4-(Dimethylamino)phenyl)-1-(4-(2-(hydroxyethoxy)ethoxy)phenyl)-2-propen-1-one (6b). The reaction described above to prepare **6a** was used, and **6b** was obtained from **5** and ethylene glycol mono-2-chloroethyl ether. ^{1}H NMR ($CDCl_3$) δ: 3.05 (s, 6H), 3.69 (t, $J = 4.8$ Hz, 2H), 3.78 (s, 2H), 3.91 (t, $J = 4.8$ Hz, 2H), 4.23 (t, $J = 4.8$ Hz, 2H), 6.70 (d, $J = 9.0$ Hz, 2H), 6.99 (d, $J = 9.0$ Hz, 2H), 7.35 (d, $J = 15.3$ Hz, 1H), 7.55 (d, $J = 8.7$ Hz, 2H), 7.79 (d, $J = 15.6$ Hz, 1H), 8.02 (d, $J = 9.0$ Hz, 2H).

(*E*)-3-(4-(Dimethylamino)phenyl)-1-(4-(2-((hydroxyethoxy)ethoxy)ethoxy)phenyl)-2-propen-1-one (6c). The reaction described above to prepare **6a** was used, and 429 mg of **6c** was obtained in a yield of 82.6% from **5** and 2-[2-(2-chloroethoxy)-ethoxy]ethanol. ^{1}H NMR ($CDCl_3$) δ: 3.04 (s, 6H), 3.62 (t, $J = 5.1$ Hz, 2H), 3.73−3.75 (m, 6H), 3.90 (t, $J = 4.8$ Hz, 2H), 4.22 (t, $J = 4.8$ Hz, 2H), 6.70 (d, $J = 9.0$ Hz, 2H), 6.99 (d, $J = 8.7$ Hz, 2H), 7.35 (d, $J = 15.3$ Hz, 1H), 7.55 (d, $J = 9.0$ Hz, 2H), 7.78 (d, $J = 15.3$ Hz, 1H), 8.02 (d, $J = 9.0$ Hz, 2H).

(*E*)-3-(4-(Dimethylamino)phenyl)-1-(4-(2-fluoroethoxy)phenyl)-2-propen-1-one (7a). To a solution of **6a** (100 mg, 0.32 mmol in 1,2-dimethoxyethane (DME) (5 mL) was added DAST (85 μL, 0.64 mmol) in a dry ice−acetone bath. The reaction mixture was stirred for 1 h at room temperature and then poured into a saturated $NaHSO_3$ solution and extracted with chloroform. After the organic phase was separated, dried over Na_2SO_4, and filtered, and the residue was purified by preparative TLC (hexane:ethyl acetate = 3:1) to give 39 mg of **7a** (38.9%). ^{1}H NMR ($CDCl_3$) δ: 3.09 (s, 6H), 4.30 (d, t, $J_1 = 27.6$ Hz, $J_2 = 4.2$ Hz, 2H), 4.79 (d, t, $J_1 = 47.4$ Hz, $J_2 = 4.2$ Hz, 2H), 6.70 (d, $J = 8.7$ Hz, 2H), 7.00 (d, $J = 9.0$ Hz, 2H), 7.35 (d, $J = 15.6$ Hz, 1H), 7.55 (d, $J = 9.0$ Hz, 2H), 7.79 (d, $J = 15.3$ Hz, 1H), 8.03 (d, $J = 9.0$ Hz, 2H). EI-MS: m/z 313 (M^+).

(*E*)-3-(4-(Dimethylamino)phenyl)-1-(4-(2-(fluoroethoxy)ethoxy)-phenyl)-2-propen-1-one (7b). The reaction described above to prepare **7a** was used, and 28 mg of **7b** was obtained in a yield of 28.0% from **6b**. ^{1}H NMR ($CDCl_3$) δ: 3.04 (s, 6H), 3.77−3.94 (m, 4H), 4.21−4.24 (m, 3H), 4.61 (d, t, $J_1 = 47.4$ Hz, $J_2 = 4.2$ Hz 1H), 6.69 (d, $J = 9.3$ Hz, 2H), 6.99 (d, $J = 8.7$ Hz, 2H), 7.35 (d, $J = 15.3$ Hz, 2H), 7.55 (d, $J = 9.0$ Hz, 2H), 7.78 (d, $J = 15.6$ Hz, 2H), 8.02 (d, $J = 9.0$ Hz, 2H). EI-MS: m/z 357 (M^+).

(*E*)-3-(4-(Dimethylamino)phenyl)-1-(4-(2-((fluoroethoxy)ethoxy)-ethoxy)phenyl)-2-propen-1-one (7c). The reaction described above to prepare **7a** was used, and 29 mg of **7c** was obtained in a yield of 14.4% from **6c** and 2-[2-(2-chloroethoxy)ethoxy]ethanol. ^{1}H NMR ($CDCl_3$) δ: 3.04 (s, 6H), 3.73−3.81 (m, 6H), 3.90 (t, $J = 5.1$ Hz, 2H), 4.21 (t, $J = 5.1$ Hz, 2H), 4.49 (t, $J = 4.5$ Hz, 1H), 4.65 (t, $J = 4.5$ Hz, 1H), 6.70 (d, $J = 8.7$ Hz, 2H), 6.98 (d, $J = 9.0$ Hz, 2H), 7.35 (d, $J = 15.3$ Hz, 1H), 7.55 (d, $J = 8.7$ Hz, 2H), 7.78 (d, $J = 15.3$ Hz, 1H), 8.02 (d, $J = 9.0$ Hz, 2H). EI-MS: m/z 401 (M^+).

1-(4-(2-Hydroxyethoxy)phenyl)ethanone (8a). The reaction described above to prepare **6a** was used, and 1.79 g of **8a** was obtained in a yield of 99.4% from 4-hydroxyacetophenone and ethylene chlorohydrin. ^{1}H NMR ($CDCl_3$) δ: 2.75 (s, 3H), 4.20 (s, 2H), 4.35 (t, $J = 5.1$ Hz, 2H), 7.15 (d, $J = 9.0$ Hz, 2H), 8.13 (d, $J = 9.0$ Hz, 2H).

1-(4-(2-(2-Hydroxyethoxy)ethoxy)phenyl)ethanone (8b). The reaction described above to prepare **6b** was used, and **8b** was obtained from 4-hydroxyacetophenone and ethylene glycol mono-2-chloroethyl ether. ^{1}H NMR ($CDCl_3$) δ: 2.56 (s, 3H), 3.68 (t, $J = 4.8$ Hz 2H), 3.75−3.79 (m, 2H) 3.90 (t, $J = 5.1$ Hz, 2H), 4.21 (t, $J = 4.8$ Hz, 2H), 6.96 (d, $J = 8.7$ Hz, 2H), 7.94 (d, $J = 8.7$ Hz, 2H).

1-(4-(2-(2-(2-Hydroxyethoxy)ethoxy)ethoxy)phenyl)ethanone (8c). The reaction described above to prepare **6a** was used, and **8c** was obtained from 4-hydroxyacetophenone and 2-[2-(chloro-ethoxy)ethoxy]ethanol. ^{1}H NMR ($CDCl_3$) δ: 2.50 (s, 3H), 3.72−3.83 (m, 6H), 3.92 (t, $J = 4.5$ Hz, 2H), 4.22 (t, $J = 5.1$ Hz, 2H), 4.49 (t, $J = 4.2$ Hz, 1H), 4.61 (t, $J = 4.2$ Hz, 1H), 6.86 (d, $J = 8.7$ Hz, 2H), 7.80 (d, $J = 8.7$ Hz, 2H).

1-(4-(2-Fluoroethoxy)phenyl)ethanone (9a). The reaction described above to prepare **7a** was used, and 1.02 g of **9a** was obtained

in a yield of 63.3% from **8a** and DAST. ^{1}H NMR ($CDCl_3$) δ: 4.24 (d, t, J_1 = 28.2 Hz, J_2 = 4.2 Hz, 2H), 4.75 (d, t, J_1 = 47.1 Hz, J_2 = 3.9 Hz, 2H), 6.92 (d, J = 9.0 Hz, 2H), 7.89 (d, J = 9.3 Hz, 2H).

1-(4-(2-(2-Fluoroethoxy)ethoxy)phenyl)ethanone (9b). The reaction described above to prepare **7b** was used, and **9b** was obtained from **9a** and DAST. ^{1}H NMR ($CDCl_3$) δ: 2.56 (s, 3H), 3.78 (t, J = 3.3 Hz, 1H), 3.86–3.94 (m, 3H), 4.22 (t, J = 5.1 Hz, 2H), 4.51 (t, J = 3.0 Hz, 1H), 4.67 (t, J = 3.0.Hz, 1H), 6.96 (d, J = 8.7 Hz, 2H), 7.93 (d, J = 8.7 Hz, 2H). EI-MS: m/z 226 (M^+).

1-(4-(2-(2-(2-Fluoroethoxy)ethoxy)ethoxy)phenyl)ethanone (9c). The reaction described above to prepare **7c** was used, and 543 mg of **9c** was obtained from **8c** and DAST. ^{1}H NMR ($CDCl_3$) δ: 2.56 (s, 3H), 3.69–3.81 (m, 6H), 3.90 (t, J = 4.5 Hz, 2H), 4.21 (t, J = 5.1 Hz, 2H), 4.49 (t, J = 4.2 Hz, 1H), 4.65 (t, J = 4.2 Hz, 1H), 6.95 (d, J = 9.3 Hz, 2H), 7.92 (d, J = 9.0 Hz, 2H). EI-MS: m/z 270 (M^+).

(*E*)-1-(4-(2-Fluoroethoxy)phenyl)-3-(4-nitrophenyl)-2-propen-1-one (10a). The reaction described above to prepare **5** was used, and 856 mg of **10a** was obtained in a yield of 56.6% from **9a** and 4-nitrobenzaldehyde. ^{1}H NMR ($CDCl_3$) δ: 4.32 (d, t, J_1 = 27.6 Hz, J_2 = 4.2 Hz, 2H), 4.81 (d, t, J_1 = 47.4 Hz, J_2 = 4.2 Hz, 2H), 7.04 (d, J = 8.7 Hz, 2H), 7.65 (d, J = 15.6 Hz, 1H), 7.79 (d, J = 8.7 Hz, 2H), 7.82 (d, J = 12.6 Hz, 1H), 8.06 (d, J = 9.0 Hz, 2H), 8.28 (d, J = 8.7 Hz, 2H).

(*E*)-1-(4-(2-(Fluoroethoxy)ethoxy)phenyl)-3-(4-nitrophenyl)-2-propen-1-one (10b). The reaction described above to prepare **5** was used, and 128 mg of **10b** was obtained from **9b** and 4-nitrobenzaldehyde. ^{1}H NMR ($CDCl_3$) δ: 3.79 (t, J = 4.2 Hz, 1H), 3.88–4.27 (m, 3H), 4.8 (t, J = 4.8 Hz, 2H), 4.53 (t, J = 4.2 Hz, 1H), 4.69 (t, J = 4.2 Hz, 1H), 7.03 (d, J = 8.7 Hz, 2H), 7.66 (d, J = 15.6 Hz, 1H), 7.79 (d, J = 9.0 Hz, 2H), 7.81 (d, J = 15.6 Hz, 1H), 8.05 (d, J = 8.7 Hz, 2H), 8.28 (d, J = 9.0 Hz, 2H).

(*E*)-1-(4-(2-((Fluoroethoxy)ethoxy)ethoxy)phenyl)-3-(4-nitrophenyl)-2-propen-1-one (10c). The reaction described above to prepare **5** was used, and 649 mg of **10c** was obtained from **9c**. ^{1}H NMR ($CDCl_3$) δ: 3.71–3.82 (m, 6H), 3.92 (t, J = 4.5 Hz, 2H), 4.24 (t, J = 4.8 Hz, 2H), 4.50 (t, J = 4.2 Hz, 1H), 4.66 (t, J = 4.5 Hz, 1H), 7.03 (d, J = 9.3 Hz, 2H), 7.66 (d, J = 15.6 Hz, 1H), 7.79 (d, J = 9.0 Hz, 2H), 7.81 (d, J = 15.6 Hz, 1H), 8.05 (d, J = 9.3 Hz, 2H), 8.28 (d, J = 8.7 Hz, 2H).

(*E*)-3-(4-Aminophenyl)-1-(4-(2-fluoroethoxy)phenyl)-2-propen-1-one (11a). A mixture of **10a** (856 mg, 2.7 mmol), $SnCl_2$ (2.55 g, 13.5 mmol), and EtOH (10 mL) was stirred at 100 °C for 2 h. After the mixture had cooled to room temperature, 1 M NaOH (10 mL) was added. The mixture was then extracted with ethyl acetate (10 mL). The organic phase was dried over Na_2SO_4 and filtered. The solvent was removed, and the residue was purified by silica gel chromatography using chloroform as a mobile phase to give 333 mg of **11a** (43.0%). ^{1}H NMR ($CDCl_3$) δ: 4.02 (s, broad, 2H), 4.30 (d, t, J_1 = 27.6 Hz, J_2 = 4.2 Hz, 2H), 4.79 (d, t, J_1 = 47.4 Hz, J_2 = 4.2 Hz, 2H), 6.68 (d, J = 8.7 Hz, 2H), 7.00 (d, J = 8.7 Hz, 2H), 7.36 (d, J = 15.3 Hz, 1H), 7.48 (d, J = 8.4 Hz, 2H), 7.75 (d, J = 15.3 Hz, 1H), 8.03 (d, J = 6.9 Hz, 2H). EI-MS: m/z 285 (M^+).

(*E*)-3-(4-Aminophenyl)-1-(4-(2-(fluoroethoxy)ethoxy)phenyl)-2-propen-1-one (11b). The reaction described above to prepare **11a** was used, and 85 mg of **11b** was obtained from **10b**. ^{1}H NMR ($CDCl_3$) δ: 3.77–3.94 (m, 4H), 4.00 (s, broad, 2H), 4.23 (t, J = 4.5 Hz, 2H), 4.53 (t, J = 4.2 Hz, 1H), 4.69 (t, J = 4.2 Hz, 1H), 6.68 (d, J = 8.4 Hz, 2H), 6.99 (d, J = 8.7 Hz, 2H), 7.74 (d, J = 15.6 Hz, 1H), 7.48 (d, J = 8.4 Hz, 1H), 7.36 (d, J = 15.3 Hz, 1H), 8.01 (d, J = 9.0 Hz, 2H). EI-MS: m/z 329 (M^+).

(*E*)-3-(4-Aminophenyl)-1-(4-(2-((fluoroethoxy)ethoxy)ethoxy)-phenyl)-2-propen-1-one (11c). The reaction described above to prepare **11a** was used, and 206 mg of **11c** was obtained from **10c**. ^{1}H NMR ($CDCl_3$) δ: 3.70–3.83 (m, 6H), 3.89 (t, J = 4.5 Hz, 2H), 4.12 (s, broad, 2H), 4.21 (t, J = 4.8 Hz, 2H), 4.49 (t, J = 4.0 Hz, 1H), 4.65 (t, J = 3.9 Hz, 1H), 6.67 (d, J = 8.7 Hz, 2H), 6.98 (d, J = 8.7 Hz, 2H), 7.36 (d, J = 15.3 Hz, 1H), 7.47 (d, J = 8.4 Hz, 2H), 7.74 (d, J = 15.9 Hz, 1H), 8.01 (d, J = 9.0 Hz, 2H). EI-MS: m/z 373 (M^+).

(*E*)-1-(4-(2-Fluoroethoxy)phenyl)-3-(4-(methylamino)phenyl)-2-propen-1-one (12a). To a solution of **11a** (290 mg, 1.02 mmol) in DMSO (6 mL) were added CH_3I (0.18 mL, 3.05 mmol) and anhydrous K_2CO_3 (691 mg, 5.08 mmol). The reaction mixture was stirred at room temperature for 3 h and poured into water. The mixture was extracted with ethyl acetate. The organic layers were combined and dried over Na_2SO_4. Evaporation of the solvent afforded a residue, which was purified by silica gel chromatography (hexane:ethyl acetate = 2:1) to give 90 mg of **12a** (29.5%). ^{1}H NMR ($CDCl_3$) δ: 2.89 (s, 3H), 4.23 (d, t, J_1 = 27.9 Hz, J_2 = 4.2 Hz, 2H), 4.79 (d, t, J_1 = 47.4 Hz, J_2 = 4.2 Hz, 2H), 6.59 (d, J = 8.7 Hz, 2H), 6.99 (d, J = 9.0 Hz, 2H), 7.34 (d, J = 15.3 Hz, 1H), 7.51 (d, J = 8.4 Hz, 2H), 7.78 (d, J = 15.3 Hz, 1H), 8.02 (d, J = 9.3 Hz, 2H). EI-MS: m/z 299 (M^+).

(*E*)-1-(4-(2-(Fluoroethoxy)ethoxy)phenyl)-3-(4-(methylamino)-phenyl)-2-propen-1-one (12b). The reaction described above to prepare **12a** was used, and 22 mg of **12b** was obtained from **11b**. ^{1}H NMR ($CDCl_3$) δ: 2.90 (s, 3H), 3.78–3.95 (m, 4H), 3.99 (s, broad, 1H), 4.23 (t, J = 4.5 Hz, 2H), 4.53 (t, J = 4.5 Hz, 2H), 4.53 (t, J = 4.2 Hz, 1H), 4.69 (t, J = 4.2 Hz, 1H), 6.60 (d, J = 8.7 Hz, 2H), 6.99 (d, J = 8.7 Hz, 2H), 7.35 (d, J = 15.3 Hz, 1H), 7.51 (d, J = 8.7 Hz, 2H), 7.77 (d, J = 15.3 Hz, 1H), 8.02 (d, J = 8.7 Hz, 2H). EI-MS: m/z 343 (M^+).

(*E*)-1-(4-(2-((Fluoroethoxy)ethoxy)ethoxy)phenyl)-3-(4-(methylamino)phenyl)-2-propen-1-one (12c). The reaction described above to prepare **12a** was used, and 53 mg of **12c** was obtained from **11c**. ^{1}H NMR ($CDCl_3$) δ: 2.89 (s, 3H), 3.69–3.83 (m, 6H), 3.90 (t, J = 4.8 Hz, 2H), 4.12 (s, broad, 1H), 4.22 (t, J = 5.1 Hz, 2H), 4.49 (t, J = 4.2 Hz, 1H), 4.65 (t, J = 4.1 Hz, 1H), 6.60 (d, J = 8.7 Hz, 2H), 6.98 (d, J = 9.0 Hz, 2H), 7.35 (d, J = 15.3 Hz, 1H), 7.51 (d, J = 8.7 Hz, 2H), 7.76 (d, J = 15.3 Hz, 1H), 8.01 (d, J = 8.7 Hz, 2H). EI-MS: m/z 387 (M^+).

(*E*)-3-(4-Dimethylaminophenyl)-1-(4-fluorophenyl)-2-propen-1-one (13). The reaction described above to prepare **5** was used, and 209 mg of **13** was obtained from 4-fluoroacetophenone and 4-dimethylbenzaldehyde. ^{1}H NMR (300 MHz, $CDCl_3$) δ: 3.03 (s, 6H), 6.68 (d, J = 8.7 Hz, 2H), 7.15 (t, J = 8.4 Hz, 2H), 7.30 (d, J = 15.3 Hz, 1H), 7.54 (d, J = 9.0 Hz, 2H), 7.78 (d, J = 15.3 Hz, 1H), 8.02–8.06 (m, 2H). EI-MS: m/z 269 (M^+).

(*E*)-1-(4-Fluorophenyl)-3-(4-nitrophenyl)-2-propen-1-one (14). The reaction described above to prepare **5** was used, and 490 mg of **14** was obtained from 4-fluoroacetophenone and 4-nitrobenzaldehyde. ^{1}H NMR (300 MHz, $CDCl_3$) δ: 7.21 (t, J = 8.7 Hz, 2H), 7.62 (d, J = 15.9 Hz, 1H), 7.80 (d, J = 8.7 Hz, 2H), 7.84 (d, J = 15.9 Hz, 1H), 8.07–8.12 (m, 2H), 8.29 (d, J = 8.7 Hz, 2H). EI-MS: m/z 271 (M^+).

(*E*)-3-(4-Aminophenyl)-1-(4-fluorophenyl)-2-propen-1-one (15). The reaction described above to prepare **11(a–c)** was used, and 150 mg of **15** was obtained from **14**. ^{1}H NMR (300 MHz, $CDCl_3$) δ: 4.07 (s, broad, 2H), 6.67 (d, J = 8.7 Hz, 2H), 7.15 (t, J = 8.7 Hz, 2H), 7.31 (d, J = 15.6 Hz, 1H), 7.47 (d, J = 8.4 Hz, 2H), 7.75 (d, J = 15.6 Hz, 1H), 8.03 (t, J = 8.7 Hz, 2H). EI-MS: m/z 241 (M^+).

(*E*)-1-(4-Fluorophenyl)-3-(4-methylaminophenyl)-2-propen-1-one (16). The reaction described above to prepare **12(a–c)** was used, and 14 mg of **16** was obtained from **15**. ^{1}H NMR (300 MHz, $CDCl_3$) δ: 2.90 (s, 3H), 4.20 (s, broad, 1H), 6.60 (d, J = 8.7 Hz, 2H), 7.17 (d, J = 8.7 Hz, 2H), 7.30 (d, J = 15.6 Hz, 1H), 7.50 (d, J = 8.7 Hz, 2H), 7.78 (d, J = 15.6 Hz, 1H), 8.04 (d, J = 8.7 Hz, 2H). EI-MS: m/z 255 (M^+).

(*E*)-2-(2-(2-(4-(3-(4-(Dimethylamino)phenyl)acryloyl)phenoxy)-ethoxy)ethoxy)ethyl 4-methylbenzenesulfonate (17). To a solution of **6c** (108 mg, 0.27 mmol) in pyridine (3 mL) was added tosyl chloride (343.8 mg, 0.621 mmol). The reaction mixture was stirred for 3 h at room temperature. After water was added, the mixture was extracted with ethyl acetate. The organic layer was dried over Na_2SO_4, and evaporation of the solvent afforded a residue, which was purified by preparative TLC (hexane:ethyl acetate = 1:1) to give 44 mg of **17** (29.4%). ^{1}H NMR (300 MHz, $CDCl_3$) δ: 2.43 (s, 3H), 3.04 (s, 6H), 3.62–3.72 (m, 6H),

3.85−3.87 (m, 2H), 4.15−4.18 (m, 4H), 6.70 (d, J = 8.7 Hz, 2H), 6.98 (d, J = 9.0 Hz, 2H), 7.31−7.35 (m, 2H), 7.37 (d, J = 9.0 Hz, 1H), 7.55 (d, J = 8.7 Hz, 2H), 7.80 (t, J = 8.7 Hz, 3H), 8.02 (d, J = 9.0 Hz, 2H). EI-MS m/z 553 (M^+)

Radiolabeling. Procedure for Labeling of 7a, 7b, 7c, and 13 with ^{11}C. ^{11}C was produced via a ^{14}N(p,α)^{11}C reaction with 16 MeV protons on a target of nitrogen gas with an ultracompact cyclotron (CYPRIS model 325R; Sumitomo Heavy Industry Ltd.) The $^{11}CO_2$ produced was transported to an automated system for the synthesis of ^{11}C-methyl iodide (CUPID C-100; Sumitomo Heavy Industry Ltd.) and converted sequentially to [^{11}C]MeOTf by the previously described method of Jewett.[33] [^{11}C]Chalcones were produced by reacting [^{11}C]MeOTf with the normethyl precursor, **7a**, **7b**, **7c**, and **13**, (0.5 mg) in 500 μL of methyl ethyl ketone (MEK). After the complete transfer of [^{11}C]MeOTf, ^{11}C-methylation was carried out for 5 min and the reaction solvent was then dried with a stream of nitrogen gas. The residue taken up in 200 μL of acetonitrile was purified by a reverse phase HPLC system (a Shimadzu LC-6A isocratic pump, a Shimadzu SPD-6A UV detector, and a Aloka NDW-351D scintillation detector) on a Cosmosil C_{18} column (Nakalai Tesque, 5C_{18}-AR-II, 10 mm × 250 mm) with an isocratic solvent of acetonitrile/water (55/45) at a flow rate of 6.0 mL/min. The desired fraction was collected in a flask and evaporated dry. The radiochemical yield, purity, and specific activity of [^{11}C]chalcones were further confirmed by analytical reverse phase HPLC on a 5C_{18}-AR-300 column (Nakalai Tesque, 4.6 mm × 150 mm, acetonitrile/water (60/40), 1.0 mL/min).

Procedure for Labeling 7c with ^{18}F. [^{18}F]Fluoride was produced by the JSW typeBC3015 cyclotron via an ^{18}O(p,n)^{18}F reaction and passed through a Sep-Pak Light QMA cartridge (Waters) as an aqueous solution in ^{18}O-enriched water. The cartridge was dried by airflow, and the ^{18}F activity was eluted with 0.5 mL of a Kryptofix 222/K_2CO_3 solution (11 mg of Kryptofix 222 and 2.6 mg of K_2CO_3 in acetonitrile/water (86/14)). The solvent was removed at 120 °C under a stream of argon gas. The residue was azeotropically dried with 1 mL of anhydrous acetonitrile twice at 120 °C under a stream of nitrogen gas and dissolved in DMSO (1 mL). A solution of tosylate precursor **17** (1.0 mg) in DMSO (1 mL) was added to the reaction vessel containing the ^{18}F activity in DMSO. The mixture was heated at 160 °C for 5 min. Water (5 mL) was added, and the mixture was passed through a preconditioned Oasis HLB cartridge (3 cm^3) (Waters). The cartridge was washed with 10 mL of water, and the labeled compound was eluted with 2 mL of acetonitrile. The eluted compound was purified by preparative HPLC [YMC-Pack Pro C_{18} column (20 mm × 150 mm), acetonitrile/water (75/25), flow rate 9.0 mL/min]. The retention time of the major byproduct of hydrolysis (t_R = 2.7 min) was well-resolved from the desired ^{18}F-labeled product (t_R = 10.7 min). The radiochemical purity and specific activity were determined by analytical HPLC [YMC-Pack Pro C_{18} column (4.6 mm × 150 mm), acetonitrile/water (60/40), flow rate 1.0 mL/min], and [^{18}F]**7c** was obtained in a radiochemical purity of >99% with the specific activity of 35 GBq/mmol. Specific activity was estimated by comparing the UV peak intensity of the purified ^{18}F-labeled compound with a reference nonradioactive compound of known concentration.

Binding Assays Using the Aggregated Aβ peptides in Solution. Aβ(1−42) was purchased from Peptide Institute (Osaka, Japan). Aggregation was carried out by gently dissolving the peptide (0.25 mg/mL) in a buffer solution (pH 7.4) containing 10 mM sodium phosphate and 1 mM EDTA. The solution was incubated at 37 °C for 42 h with gentle and constant shaking. Binding experiments were carried out as described previously.[18] [^{125}I]DMIC with 2200 Ci/mmol of specific activity and radiochemical purity greater than 95% was prepared using the standard iododestannylation reaction. A mixture containing 50 μL of test compound (0.2 pM-400 μM in 10% EtOH), 50 μL of 0.02 nM [^{125}I]DMIC, 50 μL of Aβ(1−42) aggregates, and 850 μL of 10% EtOH was incubated at room temperature for 3 h. The mixture was then filtered through Whatman GF/B filters using a Brandel M-24 cell harvester, and the radioactivity of the filters containing the bound ^{125}I ligand was measured in a γ counter. Values for the half-maximal inhibitory concentration (IC_{50}) were determined from displacement curves of three independent experiments using GraphPad Prism 4.0, and those for the inhibition constant (K_i) were calculated using the Cheng−Prusoff equation: $K_i = IC_{50}/(1 + [L]/K_d)$, where [L] is the concentration of [^{125}I]DMIC used in the assay and K_d is the dissociation constant of DMIC (4.2 nM).[19] DMIC and IMPY used as test compounds for the inhibition assay were synthesized as reported previously.[19,34]

Biodistribution in Normal Mice. Experiments with animals were conducted in accordance with our institutional guidelines and approved by the Nagasaki University Animal Care Committee and the Kyoto University Animal Care Committee. A 100 μL amount of a saline solution containing the radiolabeled agent (3.7 MBq), EtOH (10%), and ascorbic acid (1 mg/mL) was injected directly into the tail vein of ddY mice (5-week-old, 22−25 g). Groups of five mice were sacrificed at various post-injection time points. The organs of interest were removed and weighed, and the radioactivity was measured with an automatic γ counter (COBRAII, Packard).

Staining of Aβ Plaques in Brain Sections of Tg2576 Transgenic Mice. The Tg2576 transgenic mice (female, 20-month-old) and wild-type (female, 20-month-old) mice were used as an Alzheimer's model and an age-matched control, respectively. After the mice were sacrificed by decapitation, the brains were immediately removed and frozen in powdered dry ice. The frozen blocks were sliced into serial sections 10 μm thick. Each slide was incubated with a 50% EtOH solution (100 μM) of compound **7c** for 10 min. The sections were washed with 50% EtOH for 3 min two times. After drying, the sections were then examined using a microscope (Nikon, Eclipse 80i) equipped with a B-2A filter set (excitation, 450−490 nm; diachronic mirror, 505 nm; long-pass filter, 520 nm). Thereafter, the serial sections were also immunostained with 3,3′-diaminobenzidine (DAB) as a chromogen using monoclonal antibodies against Aβ (amyloid β-protein immunohistostain kit, WAKO).

In Vitro Autoradiography Using Human AD Brains. Postmortem brain tissues from an autopsy-confirmed case of AD (73-year-old male) were obtained from BioChain Institute Inc. The presence and localization of plaques on the sections were confirmed with immunohistochemical staining using a monoclonal Aβ antibody as described above. The sections were incubated with [^{18}F]**7c** (54 μCi/200 μL) for 1 h at room temperature. They were then washed in 50% EtOH (two 1 min wash), before being rinsed with water for 30 s. After drying, the ^{18}F-labeled sections were exposed to a BAS imaging plate (Fuji Film, Tokyo, Japan) for 6 h. Ex vivo autoradiographic images were obtained using a BAS5000 scanner system (Fuji Film). After autoradiographic examination, the same sections were stained by thioflavin-S to confirm the presence of Aβ plaques. For the staining of thioflavin-S, sections were immersed in a 0.125% thioflavin-S solution containing 50% EtOH for 3 min and washed in 50% EtOH. After drying, the sections were then examined using a microscope (Nikon, Eclipse 80i) equipped with a B-2A filter set (excitation, 450−490 nm; diachronic mirror, 505 nm; long-pass filter, 520 nm).

Acknowledgment. This study was supported by the Program for Promotion of Fundamental Studies in Health Sciences of the National Institute of Biomedical Innovation (NIBIO), a Health Labour Sciences Research Grant, and a Grant-in-Aid for Young Scientists (A) and Exploratory Research from the Ministry of Education, Culture, Sports, Science and Technology, Japan.

Supporting Information Available: Representative HPLC chromatograms of [^{18}F]**7c**. This material is available free of charge via the Internet at http://pubs.acs.org.

References

(1) Hardy, J. A.; Higgins, G. A. Alzheimer's disease: the amyloid cascade hypothesis. *Science* **1992**, *256*, 184–185.

(2) Selkoe, D. J. Alzheimer's disease: genes, proteins, and therapy. *Physiol. Rev.* **2001**, *81*, 741–766.

(3) Nordberg, A. PET imaging of amyloid in Alzheimer's disease. *Lancet Neurol.* **2004**, *3*, 519–527.

(4) Mathis, C. A.; Wang, Y.; Klunk, W. E. Imaging β-amyloid plaques and neurofibrillary tangles in the aging human brain. *Curr. Pharm. Des.* **2004**, *10*, 1469–1492.

(5) Klunk, W. E.; Engler, H.; Nordberg, A.; Wang, Y.; Blomqvist, G.; Holt, D. P.; Bergstrom, M.; Savitcheva, I.; Huang, G. F.; Estrada, S.; Ausen, B.; Debnath, M. L.; Barletta, J.; Price, J. C.; Sandell, J.; Lopresti, B. J.; Wall, A.; Koivisto, P.; Antoni, G.; Mathis, C. A.; Langstrom, B. Imaging brain amyloid in Alzheimer's disease with Pittsburgh Compound-B. *Ann. Neurol.* **2004**, *55*, 306–319.

(6) Mathis, C. A.; Wang, Y.; Holt, D. P.; Huang, G. F.; Debnath, M. L.; Klunk, W. E. Synthesis and evaluation of ^{11}C-labeled 6-substituted 2-arylbenzothiazoles as amyloid imaging agents. *J. Med. Chem.* **2003**, *46*, 2740–2754.

(7) Verhoeff, N. P.; Wilson, A. A.; Takeshita, S.; Trop, L.; Hussey, D.; Singh, K.; Kung, H. F.; Kung, M. P.; Houle, S. In vivo imaging of Alzheimer disease β-amyloid with [^{11}C]SB-13 PET. *Am. J. Geriatr. Psychiatry* **2004**, *12*, 584–595.

(8) Ono, M.; Wilson, A.; Nobrega, J.; Westaway, D.; Verhoeff, P.; Zhuang, Z. P.; Kung, M. P.; Kung, H. F. ^{11}C-Labeled stilbene derivatives as Abeta-aggregate-specific PET imaging agents for Alzheimer's disease. *Nucl. Med. Biol.* **2003**, *30*, 565–571.

(9) Small, G. W.; Kepe, V.; Ercoli, L. M.; Siddarth, P.; Bookheimer, S. Y.; Miller, K. J.; Lavretsky, H.; Burggren, A. C.; Cole, G. M.; Vinters, H. V.; Thompson, P. M.; Huang, S. C.; Satyamurthy, N.; Phelps, M. E.; Barrio, J. R. PET of brain amyloid and tau in mild cognitive impairment. *N. Engl. J. Med.* **2006**, *355*, 2652–2663.

(10) Shoghi-Jadid, K.; Small, G. W.; Agdeppa, E. D.; Kepe, V.; Ercoli, L. M.; Siddarth, P.; Read, S.; Satyamurthy, N.; Petric, A.; Huang, S. C.; Barrio, J. R. Localization of neurofibrillary tangles and β-amyloid plaques in the brains of living patients with Alzheimer disease. *Am. J. Geriatr. Psychiatry* **2002**, *10*, 24–35.

(11) Rowe, C. C.; Ackerman, U.; Browne, W.; Mulligan, R.; Pike, K. L.; O'Keefe, G.; Tochon-Danguy, H.; Chan, G.; Berlangieri, S. U.; Jones, G.; Dickinson-Rowe, K. L.; Kung, H. P.; Zhang, W.; Kung, M. P.; Skovronsky, D.; Dyrks, T.; Holl, G.; Krause, S.; Friebe, M.; Lehman, L.; Lindemann, S.; Dinkelborg, L. M.; Masters, C. L.; Villemagne, V. L. Imaging of amyloid β in Alzheimer's disease with ^{18}F-BAY94-9172, a novel PET tracer: proof of mechanism. *Lancet Neurol.* **2008**, *7*, 129–135.

(12) Zhang, W.; Oya, S.; Kung, M. P.; Hou, C.; Maier, D. L.; Kung, H. F. F-18 polyethyleneglycol stilbenes as PET imaging agents targeting Aβ aggregates in the brain. *Nucl. Med. Biol.* **2005**, *32*, 799–809.

(13) Lockhart, A. Imaging Alzheimer's disease pathology: one target, many ligands. *Drug Discovery Today* **2006**, *11*, 1093–1099.

(14) Ye, L.; Morgenstern, J. L.; Gee, A. D.; Hong, G.; Brown, J.; Lockhart, A. Delineation of positron emission tomography imaging agent binding sites on β-amyloid peptide fibrils. *J. Biol. Chem.* **2005**, *280*, 23599–235604.

(15) Lockhart, A.; Ye, L.; Judd, D. B.; Merritt, A. T.; Lowe, P. N.; Morgenstern, J. L.; Hong, G.; Gee, A. D.; Brown, J. Evidence for the presence of three distinct binding sites for the thioflavin T class of Alzheimer's disease PET imaging agents on β-amyloid peptide fibrils. *J. Biol. Chem.* **2005**, *280*, 7677–7684.

(16) Ono, M.; Yoshida, N.; Ishibashi, K.; Haratake, M.; Arano, Y.; Mori, H.; Nakayama, M. Radioiodinated flavones for in vivo imaging of β-amyloid plaques in the brain. *J. Med. Chem.* **2005**, *48*, 7253–7260.

(17) Ono, M.; Watanabe, R.; Kawashima, H.; Kawai, T.; Watanabe, H.; Haratake, M.; Saji, H.; Nakayama, M. ^{18}F-Labeled flavones for in vivo imaging of β-amyloid plaques in Alzheimer's brains. *Bioorg. Med. Chem.* **2009**, *17*, 2069–2076.

(18) Ono, M.; Hori, M.; Haratake, M.; Tomiyama, T.; Mori, H.; Nakayama, M. Structure–activity relationship of chalcones and related derivatives as ligands for detecting of β-amyloid plaques in the brain. *Bioorg. Med. Chem.* **2007**, *15*, 6388–6396.

(19) Ono, M.; Haratake, M.; Mori, H.; Nakayama, M. Novel chalcones as probes for in vivo imaging of β-amyloid plaques in Alzheimer's brains. *Bioorg. Med. Chem.* **2007**, *15*, 6802–6809.

(20) Maya, Y.; Ono, M.; Watanabe, H.; Haratake, M.; Saji, H.; Nakayama, M. Novel radioiodinated aurones as probes for SPECT imaging of β-amyloid plaques in the brain. *Bioconjugate Chem.* **2009**, *20*, 95–101.

(21) Ono, M.; Maya, Y.; Haratake, M.; Ito, K.; Mori, H.; Nakayama, M. Aurones serve as probes of β-amyloid plaques in Alzheimer's disease. *Biochem. Biophys. Res. Commun.* **2007**, *361*, 116–121.

(22) Stephenson, K. A.; Chandra, R.; Zhuang, Z. P.; Hou, C.; Oya, S.; Kung, M. P.; Kung, H. F. Fluoro-pegylated (FPEG) imaging agents targeting Aβ aggregates. *Bioconjugate Chem.* **2007**, *18*, 238–246.

(23) Qu, W.; Kung, M. P.; Hou, C.; Oya, S.; Kung, H. F. Quick assembly of 1,4-diphenyltriazoles as probes targeting β-amyloid aggregates in Alzheimer's disease. *J. Med. Chem.* **2007**, *50*, 3380–3387.

(24) Zhang, W.; Oya, S.; Kung, M. P.; Hou, C.; Maier, D. L.; Kung, H. F. F-18 stilbenes as PET imaging agents for detecting β-amyloid plaques in the brain. *J. Med. Chem.* **2005**, *48*, 5980–5988.

(25) Kung, M. P.; Hou, C.; Zhuang, Z. P.; Zhang, B.; Skovronsky, D.; Trojanowski, J. Q.; Lee, V. M.; Kung, H. F. IMPY: an improved thioflavin-T derivative for in vivo labeling of β-amyloid plaques. *Brain Res.* **2002**, *956*, 202–210.

(26) Hsiao, K.; Chapman, P.; Nilsen, S.; Eckman, C.; Harigaya, Y.; Younkin, S.; Yang, F.; Cole, G. Correlative memory deficits, Aβ elevation, and amyloid plaques in transgenic mice. *Science* **1996**, *274*, 99–102.

(27) Kuntner, C.; Kesner, A. L.; Bauer, M.; Kremslehner, R.; Wanek, T.; Mandler, M.; Karch, R.; Stanek, J.; Wolf, T.; Muller, M.; Langer, O. Limitations of small animal PET imaging with [^{18}F]FDDNP and FDG for quantitative studies in a transgenic mouse model of Alzheimer's disease. *Mol. Imaging Biol.* **2009**, *11*, 236–240.

(28) Klunk, W. E.; Lopresti, B. J.; Ikonomovic, M. D.; Lefterov, I. M.; Koldamova, R. P.; Abrahamson, E. E.; Debnath, M. L.; Holt, D. P.; Huang, G. F.; Shao, L.; DeKosky, S. T.; Price, J. C.; Mathis, C. A. Binding of the positron emission tomography tracer Pittsburgh compound-B reflects the amount of amyloid-β in Alzheimer's disease brain but not in transgenic mouse brain. *J. Neurosci.* **2005**, *25*, 10598–10606.

(29) Maeda, J.; Ji, B.; Irie, T.; Tomiyama, T.; Maruyama, M.; Okauchi, T.; Staufenbiel, M.; Iwata, N.; Ono, M.; Saido, T. C.; Suzuki, K.; Mori, H.; Higuchi, M.; Suhara, T. Longitudinal, quantitative assessment of amyloid, neuroinflammation, and anti-amyloid treatment in a living mouse model of Alzheimer's disease enabled by positron emission tomography. *J. Neurosci.* **2007**, *27*, 10957–10968.

(30) Toyama, H.; Ye, D.; Ichise, M.; Liow, J. S.; Cai, L.; Jacobowitz, D.; Musachio, J. L.; Hong, J.; Crescenzo, M.; Tipre, D.; Lu, J. Q.; Zoghbi, S.; Vines, D. C.; Seidel, J.; Katada, K.; Green, M. V.; Pike, V. W.; Cohen, R. M.; Innis, R. B. PET imaging of brain with the β-amyloid probe, [^{11}C]6-OH-BTA-1, in a transgenic mouse model of Alzheimer's disease. *Eur. J. Nucl. Med. Mol. Imaging* **2005**, *32*, 593–600.

(31) Skovronsky, D. M.; Zhang, B.; Kung, M. P.; Kung, H. F.; Trojanowski, J. Q.; Lee, V. M. In vivo detection of amyloid plaques in a mouse model of Alzheimer's disease. *Proc. Natl. Acad. Sci. U.S.A* **2000**, *97*, 7609–7614.

(32) Saido, T. C.; Iwatsubo, T.; Mann, D. M.; Shimada, H.; Ihara, Y.; Kawashima, S. Dominant and differential deposition of distinct β-amyloid peptide species, A β N3(pE), in senile plaques. *Neuron* **1995**, *14*, 457–466.

(33) Jewett, D. M. A simple synthesis of [^{11}C]methyl triflate. *Int. J. Radiat. Appl. Instrum. A* **1992**, *43*, 1383–1385.

(34) Zhuang, Z. P.; Kung, M. P.; Wilson, A.; Lee, C. W.; Plossl, K.; Hou, C.; Holtzman, D. M.; Kung, H. F. Structure–activity relationship of imidazo[1,2-*a*]pyridines as ligands for detecting β-amyloid plaques in the brain. *J. Med. Chem.* **2003**, *46*, 237–243.

—Reviews—

PET/SPECTによる分子イメージング研究

小野正博

Molecular Imaging by PET/SPECT

Masahiro ONO

Department of Patho-Functional Bioanalysis, Graduate School of Pharmaceutical Sciences, Kyoto University, 46–29 Yoshida Shimoadachi-cho, Sakyo-ku, Kyoto 606–8501, Japan

(Received September 19, 2008)

Molecular imaging by PET/SPECT with radiopharmaceuticals enables noninvasively quantitative evaluation of physiological function, gene expression, pharmacokinetics of proteins and peptides and distribution of receptors with high sensitivity. Together with recent development of imaging equipments, molecular imaging by PET/SPECT is expected to contribute to elucidation of physiological and pathological functions, medical sciences and clinical diagnoses. Molecular imaging with radiopharmaceuticals started from diagnosis of cancer with ^{18}F-2-fluoro-2-deoxyglucose ([^{18}F]FDG). Currently, [^{18}F]FDG is commonly used in the field of clinical diagnosis, because it can provide qualitative information on malignancy and metastasis of tumor. Since its achievement, much effort has been devoted to the development of radiopharmaceuticals that bind or interact with the *in vivo* biomarkers. For example, a number of radiopharmaceuticals based on proteins and peptides with high binding affinities to various biomarkers have been applied for the diagnosis of tumor, arteriosclerosis, thrombus and so on. Furthermore, Alzheimer's disease is also a major target for diagnosis by PET/SPECT imaging. The development of low-molecular-weight radiolabeled probes for the quantitation of β-amyloid plaques and neurofibrillary tangles in Alzheimer's brains is a topic of current PET/SPECT imaging studies. Here, some recent progress and development of radiopharmaceuticals for PET/SPECT imaging will be reviewed.

Key words——molecular imaging; radiopharmaceutical; tumor; positron emission tomography (PET); single photon emission computed tomography (SPECT); β-amyloid

1. はじめに

体内における遺伝子やタンパク質などの分子を生物が生きたままの状態で画像化する「分子イメージング」は，様々な病態に関与する分子を画像化することで疾患の高度な診断を可能にすると考えられている．分子イメージングには，PET (positron emission tomography)/SPECT (single photon emission computed tomography)，光イメージング，磁気共鳴イメージング (MRI) などが汎用されているが，中でもPET/SPECTによる分子イメージングは，放射性核種 (radioisotope, RI) で標識した放射性化合物を生体内に投与し，標的部位に分布あるいは標的分子に結合した放射性化合物から放出されるガンマ線を体外より検出，定量画像化する技術である．このような特徴を生かして，PET/SPECTによる分子イメージングは現在，生体機能の病因の解明，再生医療，テーラーメード医療などの医学研究，創薬研究，臨床診断分野などへの貢献が期待されている．

PET/SPECTのインビボイメージングに用いられるRIは，ポジトロン放出核種 (PET核種) とシングルフォトン放出核種 (SPECT核種) の2種類に大別される．PET核種は，β^+ 崩壊により生成する陽電子が陰電子と結合し，511 keVの2本のガンマ線を180°方向に同時に放出する核種であり，^{11}C, ^{13}N, ^{15}O, ^{18}Fなどが用いられる．SPECT核種は，電子捕獲や核異性体転移により単一のガンマ線を放出する核種であり，インビボイメージングに用いられる核種として，^{67}Ga, ^{99m}Tc, ^{111}In, ^{123}Iなどが挙げられる．これらのPET核種の半減期は，2分から110分と非常に短いのに対して，SPECT核種は，

京都大学大学院薬学研究科病態機能分析学分野 (〒606–8501 京都市左京区吉田下阿達町 46–29)
e-mail: ono@pharm.kyoto-u.ac.jp

本総説は，日本薬学会第128年会シンポジウムS36で発表したものを中心に記述したものである．

数時間から数十時間の半減期であるという点で異なる（Table 1）.

一般的に分子イメージングプローブに求められる条件としては，合成が容易で，収率が高く，生体内に投与後，できるだけ短時間に標的部位へ移行し，高い標的／非標的比が得られること，安全性が高いことなどが挙げられる．また PET/SPECT 用分子プローブでは，さらに短半減期の核種で標識する必要があるため，1）迅速な合成ができること，2）微量でも定量的に反応が進行すること，3）高い放射化学的収率及び放射化学的純度で得られること，4）代謝の影響等を受けない部位に選択的に標識できることなどの条件も必要となる．

2. PET/SPECT による腫瘍の分子イメージング

次に，PET/SPECT を用いた腫瘍の分子イメージングについて紹介する．現在，腫瘍のイメージング剤として最も臨床で利用されているのが，[^{18}F]FDG（2-deoxy-2-[^{18}F]-fluoro-D-glucose）である（Fig. 1）．[^{18}F]FDG は，グルコースの 2 位の水酸基を ^{18}F に置換した構造をしており，グルコースと同様に，グルコーストランスポータにより，血液から細胞内に取り込まれ，ヘキソキナーゼによって 6 位リン酸化を受けるが，生成した [^{18}F]FDG-6 リン酸（2-deoxy-2-fluoro-D-glucose-6-phosphate）は，それ以降の解糖系酵素の基質とならないため細胞内に滞留する．したがって，[^{18}F]FDG の細胞内への集積はグルコーストランスポータとヘキソキナーゼの活性により決まり，グルコーストランスポータの発現とヘキソキナーゼ活性が亢進している腫瘍細胞では [^{18}F]FDG の高い集積を示し，腫瘍のイメージングが可能になる．本邦においても，2002 年 4 月から [^{18}F]FDG-PET が保険適用され，PET 検査数は急激な増加傾向にある．しかしながら，あくまで [^{18}F]FDG は，細胞のグルコース代謝を反映しており，腫瘍に特異的ではないこと，脳への生理的集積が高いこと，炎症部位にも集積することなどの問題を有しており，現在，[^{18}F]FDG より腫瘍特異性の高い分子プローブの開発が活発に行われている．これまでに，[^{18}F]FDG 以外にも，多くの PET/SPECT 用腫瘍分子イメージングプローブが報告されており，2 種類に大別される（Table 2）．1 つは，腫瘍細胞で亢進した生体機能に着目したプローブであり，核酸代謝イメージング剤，[1] アミノ酸代謝イメージング剤，[2] 膜脂質代謝イメージング剤[3] などが開発されている．もう 1 つは，腫瘍部位の組織環境・特異的発現分子に着目したプローブであり，腫瘍の低酸素部位イメージング剤である，ニトロイミダゾール誘導体，[4] 銅キレート錯体，[5] アポトーシスのイメージング剤，[6] 腫瘍細胞に多く発現したソマトスタチンレセプターを標的にした，レセプタ発現イメージング剤，[7] 血管新生の際に高い発現を示す，$\alpha_V\beta_3$ インテグリンレセプターを標的に

Table 1. Radioisotopes Used for PET/SPECT Imaging

核　種	物理的半減期	放射線エネルギー (keV)
ポジトロン放出核種		
^{11}C	20.39 m	511
^{13}N	9.96 m	511
^{15}O	122 s	511
^{18}F	109.8 m	511
シングルフォトン放出核種		
^{67}Ga	78.3 h	93, 185, 300
^{99m}Tc	6.01 h	141
^{111}In	2.81 d	171, 245
^{123}I	13.3 h	159

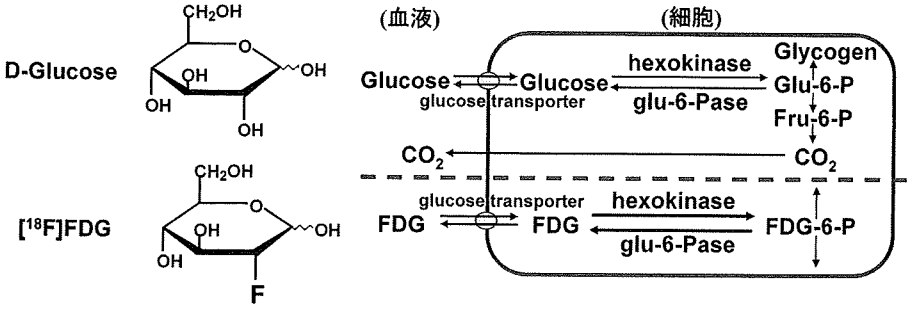

Fig. 1. Mechanism of Cellular Uptake of [^{18}F]FDG

Table 2. Tumor Imaging Probes for PET/SPECT

腫瘍細胞で亢進した生体機能に着目したプローブ	腫瘍部位の組織環境，特異的発現分子に着目したプローブ
糖代謝イメージング	低酸素部位イメージング
グルコース誘導体：[^{18}F] FDG	ニトロイミダゾール誘導体
糖代謝イメージング	[^{18}F] FMISO, [^{18}F] FAZA
核酸誘導体：[^{18}F] FLT	銅キレート化合物
アミノ酸代謝イメージング	[$^{62/64}$Cu] ATSM
アミノ酸，アミノ酸誘導体	アポトーシスイメージング
[^{11}C] メチオニン，[^{18}F] FET，[^{18}F] FAMT，[^{18}F] FACBC	[^{18}F/^{99m}Tc] annexin V
膜脂質代謝イメージング	レセプタ発現イメージング
コリン，コリン誘導体	[^{18}F/^{111}In/^{99m}Tc] オクトレオタイド
[^{18}F] フルオロコリン，[^{18}F] コリン	血管新生イメージング
	[^{18}F/^{111}In/^{99m}Tc] RGD ペプチド
	放射免疫シンチグラフィー
	[^{111}In/^{99m}Tc] 抗体，抗体フラグメント

したイメージング剤，[8] また，がん細胞表面に発現したがん抗原に対する抗体を用いる，放射免疫シンチグラフィ[9]などが知られている．[^{18}F]FDG を含めて，核酸代謝イメージング剤，アミノ酸代謝イメージング剤，膜脂質代謝イメージング剤，低酸素部位のイメージング剤は，いずれも低分子化合物であるのに対して，アポトーシスのイメージング剤，レセプタ発現イメージング剤，血管新生イメージング剤，放射免疫シンチグラフィに用いられるプローブは，タンパク質・ペプチドを基盤とするものであり，そのプローブの設計は大きく異なる．

そこで次に，タンパク質・ペプチドを基盤とした腫瘍の分子イメージングプローブについて紹介する．タンパク質・ペプチドを基盤とする分子プローブは，腫瘍指向性のタンパク質・ペプチドの標的分子の結合部位とは独立して，同一分子内に RI の結合部位を有する二官能性放射性薬剤のことを言い，腫瘍指向性のタンパク質・ペプチドが RI のキャリアとして，腫瘍部位へ放射能を送達する．腫瘍指向性のタンパク質・ペプチドとしては，抗腫瘍抗体，そのフラグメント，オクトレオタイド，RGD ペプチドなどが利用されている．この二官能性放射性薬剤の原理は，腫瘍イメージングに限らず，ほかの病態に対するタンパク質・ペプチドを使用することにより様々な病態の診断にも応用できることから，多くの放射性プローブの開発に応用されている．二官能性放射性薬剤には，SPECT 用 RI である，^{67}Ga，^{99m}Tc，^{111}In がよく使われる．しかし一般的に，金属 RI は，タンパク質・ペプチドと直接安定に結合しないため，二官能性放射性薬剤の作製には，同一分子内にタンパク質・ペプチドとの結合部位と金属 RI とのキレート形成部位とを併せ持つ，二官能性キレート試薬が必要である（Fig. 2）．

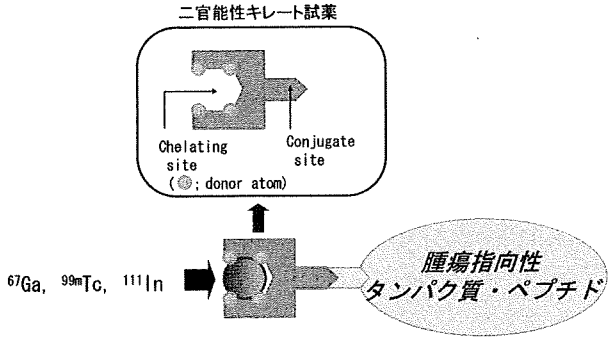

Fig. 2. Bifuctional Chelating Agents to Label Proteins and Peptides with Metal Radioiosotopes

われわれは，腫瘍のイメージングを目的とした抗腫瘍抗体 Fab フラグメントの ^{99m}Tc 標識体を作製するために，6-hydrazinonicotinamide-3-carboxylic acid (HYNIC) を二官能性キレート試薬として選択した．HYNIC は，hydrazinopyridine をキレート部位，カルボン酸を抗体フラグメントのリジン残基との結合とする化合物であり，補助配位子として，トリシンとベンゾイルピリジン（BP）を用いて，抗体 Fab フラグメントを ^{99m}Tc で標識した，^{99m}Tc-(HYNIC-Fab) (tricine) (BP) を作製し，腫瘍移植マウスを用いる検討を行った（Fig. 3）．^{99m}Tc 標識 Fab フラグ

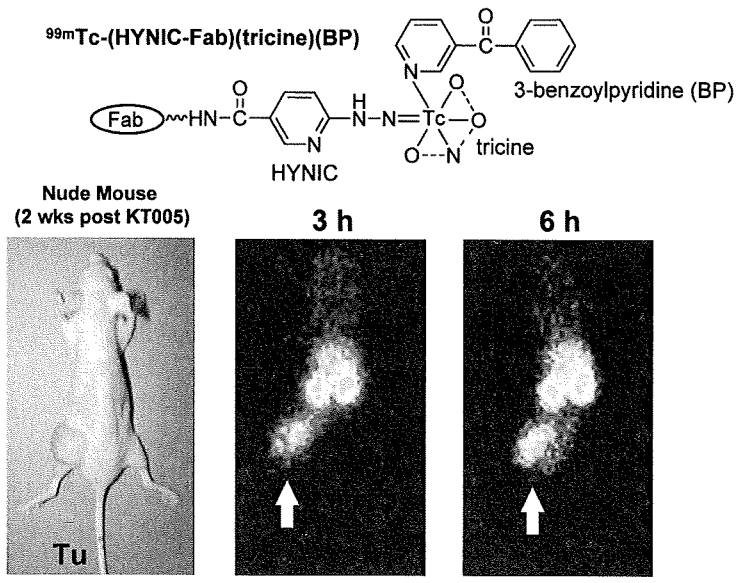

Fig. 3. Tumor Imaging in a Model Mouse with ^{99m}Tc-(HYNIC-Fab) (tricine) (BP)

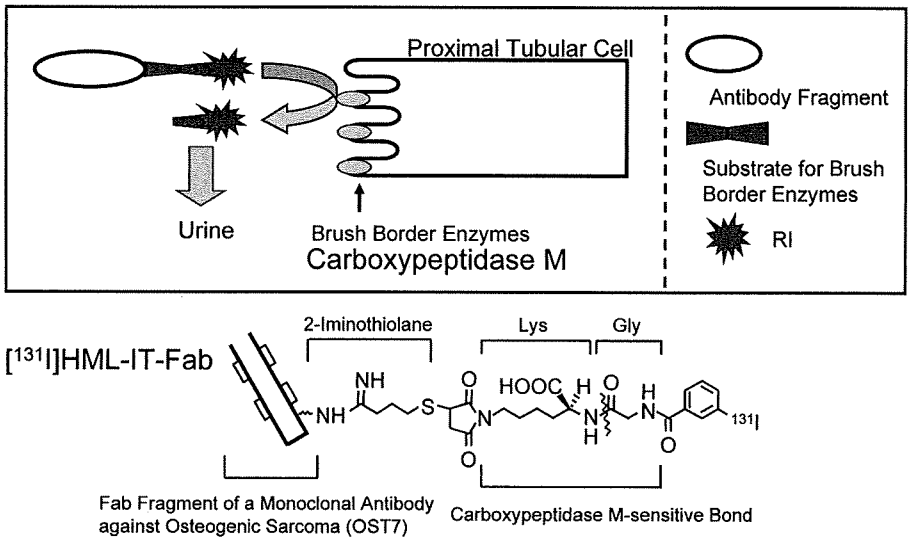

Fig. 4. Brush Border Strategy to Reduce Radioactivity Level in the Kidney

メントを腫瘍移植マウスに投与3及び6時間後の腫瘍と血液の放射能集積比とシンチグラムの結果を示した．腫瘍血液の放射能集積比は，経時的に向上し，シンチグラムにおいても，マウスの左大腿部に移植した腫瘍をイメージングすることに成功した.[10] しかし，腫瘍以外に腎臓への高い放射能滞留も観察された．このような非特異的な放射能集積は，ほかのタンパク質・ペプチドを基盤とした放射性プローブにも観察され，^{111}In 標識抗腫瘍抗体では肝臓に，^{111}In 標識オクトレオチドでは，腎臓に非常に高い放射能集積が認められ，腫瘍の診断精度の低下や不要な放射線被爆を引き起こす大きな原因となっている．

RI 標識抗体フラグメントやペプチドを生体内に投与後に観察される，腎臓における非特異的放射能集積を低減する目的で，RI 標識ポリペプチドを投与時の腎臓における放射能集積の化学制御に関する研究が行われている．その1つが，Brush Border Strategy と呼ばれる手法である（Fig. 4）．この手法は，RI 標識抗体フラグメントを生体に投与し，糸

球体ろ過を受けたのち，腎尿細管細胞に取り込まれる前に，刷子縁酵素カルボキシペプチダーゼMによって，尿排泄性の高い放射性化合物を速やかに遊離させることにより，腎臓への非特異的な放射能集積を低減させるという原理に基づいている．カルボキシペプチダーゼMにより，グリシン-リジン配列が選択的に切断されること，メタヨード馬尿酸が速やかに尿排泄されることに着目して，放射性ヨウ素標識 *m*-ヨード馬尿酸のグリシン残基をリジンのαアミノ基と結合させ，さらにそのリジン残基のεアミノ基を抗体フラグメントとの結合に有効なマレイミド基に変換した，放射性ヨウ素標識HMLが設計・合成され，このHMLを用いて放射性ヨウ素標識したFabを用いた検討が行われた.[11] その結果，^{131}I-HML-Fabを腫瘍移植マウスに投与3時間後までに，[^{131}I]m-ヨード馬尿酸が尿中に速やかに排泄されることにより，腎臓への放射能集積はほとんど観察されず，腫瘍部位の明瞭なイメージングが達成されている．今後，本手法を^{99m}Tcや^{111}Inなどの金属RIに応用することにより，抗体フラグメントを基盤とした有効な腫瘍イメージングプローブの開発が期待される．

3. PET/SPECTによる脳神経疾患の分子イメージング

次に，代表的な脳神経疾患であるアルツハイマー病のPET/SPECTによる分子イメージングについて紹介する．

アルツハイマー病に特徴的な脳内病理学的変化として，βシート構造を取ったアミロイドβペプチドからなる老人斑の沈着と過剰にリン酸化されたタウタンパクからなる神経原線維変化の出現が知られている．これら病変の中でも，老人斑の沈着は，アルツハイマー病発症過程の最も初期段階から生じる病理学的変化と考えられ，臨床症状が現れる数十年前から始まることが明らかとなっている．したがって，体外からの老人斑の検出は，アルツハイマー病の早期診断につながると考えられることから，現在，アミロイドイメージングプローブを利用した老人斑のインビボ画像診断が注目されている．

老人斑アミロイドは，アルツハイマー病脳において，アミロイド前駆タンパク質（APP）からセクレターゼβとγにより切り出されたアミロイドβペプチド（Aβ40及びAβ42）の凝集，繊維化によって生成する．この老人斑を体外より画像化するために，アミロイドイメージングプローブに求められる性質として，1）生体内へ投与後に，血液脳関門を通過すること，2）老人斑に選択的に結合し，3）老人斑アミロイドに結合しない非結合分子は速やかに脳から血液へ消失することが挙げられる．老人斑アミロイドのインビボ分子イメージングは，このような条件を満たして老人斑アミロイドに特異的に結合したアミロイドイメージングプローブから放出されるガンマ線をPET/SPECT装置を用いて体外より検出し，老人斑を画像化するという原理に基づい

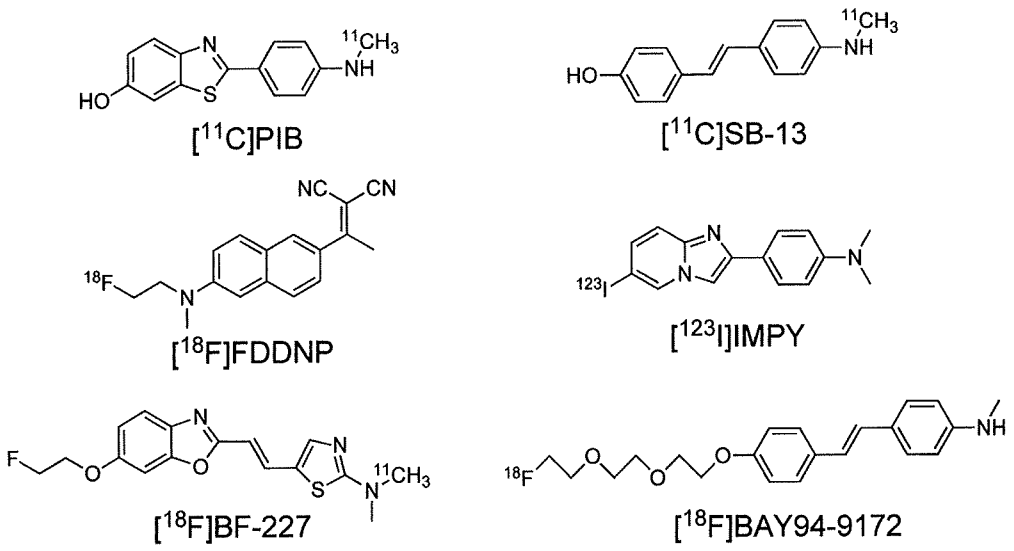

Fig. 5. Chemical Structures of β-Amyloid Imaging Probes Tested Clinically

ている．

Figure 5 には，これまでに臨床で使用されたアミロイドイメージングプローブの化学構造式を示す．[12-17] その多くが老人斑の蛍光染色試薬であるコンゴーレッド，チオフラビン T の構造を基に開発されており，^{11}C あるいは ^{18}F で標識された 5 種類の PET 用プローブ及び ^{123}I で標識された 1 種類の SPECT 用プローブが臨床評価された．PET 用プローブによる多くの臨床研究が行われ，アルツハイマー病診断におけるアミロイドイメージングの有用性が報告されてきた一方で，SPECT 診断用プローブとしては，[^{123}I] IMPY が報告されているが，脳移行後の非特異的放射能滞留が認められることから，より高性能なプローブの開発が望まれている．

現在最も多くの臨床研究が行われている [^{11}C] PIB の臨床研究の PET 撮像の結果を Fig. 6 に示した．アルツハイマー病患者の脳は，コントロールには観察されない，非常に高い放射能集積が観察され，PIB のアミロイドイメージングにより，アルツハイマー病患者と健常人との鑑別は可能であることが報告されている．[13] また，ヒトアミロイド斑には高い結合性を示す一方，マウスアミロイド斑への結合性が低いことが報告されており，[18] 最近の論文において，マウスアミロイド斑には存在せず，ヒトアミロイド斑に多く存在する *N* 末端がピログルタミン酸修飾されたアミロイド β42 への PIB の結合性が示唆されている．[19]

次に，われわれが開発した PET 用アミロイドイメージングプローブを紹介する．PIB の化学構造中のチアゾールをフランに変換した，フェニルベンゾフランを基本骨格とする，[^{11}C] HMBZF [5-hydroxy-2-(4-[^{11}C] methylaminophenyl) benzofuran] を設計・合成した．アルツハイマー病患者脳ホモジネートを用いた阻害実験を行った結果，阻害定数 (K_i) が 0.7 nM と PIB の 4.3 nM よりもアミロイドへの高い結合性を示した．正常マウスにおける体内放射能分布実験を行ったところ，投与初期の高い脳移行性とその後の速やかなクリアランスを示すことが明らかとなった．次に，アルツハイマー病モデルマウスに投与後，*ex vivo* オートラジオグラフィーを行った結果，野生型マウスに比べ，高い放射能集積が認められ，さらにこの放射能集積は，アミロイドの蛍光染色試薬チオフラビン S の染色位置と一致した (Fig. 7)．これらの結果より，HMBZF が PET 用アミロイドイメージングプローブとして有用であることが示された．[20]

前述のように，既報のアミロイドイメージングプローブは，その多くがコンゴーレッドやチオフラビン T から派生した化学構造であることから，われわれはアミロイドイメージングプローブとして機能する新たな分子骨格の探索研究を行ってきた．最近，インビトロにおいて，フラボノイド化合物にアミロイド β ペプチドの凝集，繊維化抑制作用があることが報告され，アミロイド β との結合性あるいは相互作用があることが考えられた．そこで，これら化合物の共通構造である，フラボン骨格をアミロイドイメージングプローブの新たな骨格に選択し，SPECT 用 RI であるヨウ素と種々の置換基を導入したフラボン誘導体を設計・合成し，アミロイドイ

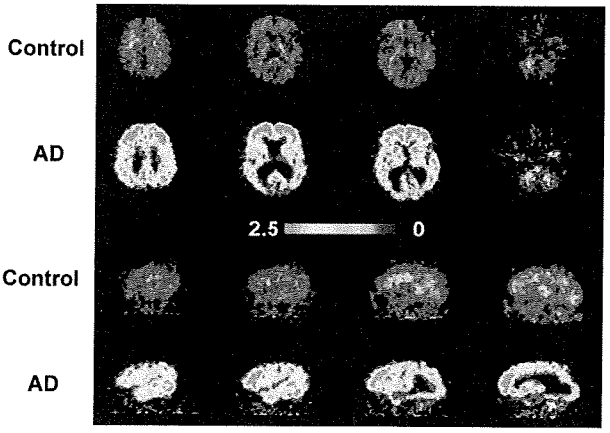

Fig. 6. [^{11}C] PIB-PET in Healty Controls and Alzheimer's Disease (AD) Patients[13]

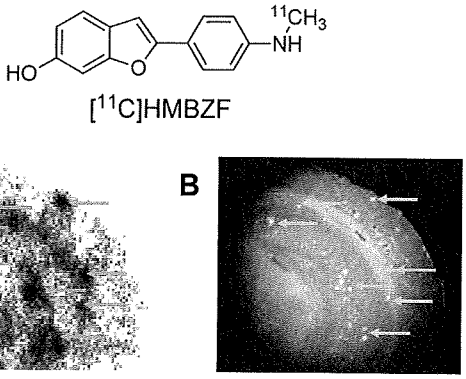

Fig. 7. *Ex vivo* Autoradiography of [^{11}C] HMBZF Using AD Model Mice (A), Thioflavin S Staining in the Same Brain Section (B)

メージングプローブとしての評価を行った（Fig. 8）．その結果，アミロイド凝集体を用いたインビトロ結合実験において，フラボン誘導体は高い結合親和性を示し，正常マウスにおける体内放射能分布実験において，フラボン誘導体は脳への高い移行性と老人斑の存在しない正常脳から速やかなクリアランスを示した．さらに，アルツハイマー病患者の脳切片を用いた検討の結果，老人斑アミロイドに高い結合性を有することが明らかとなった．これらの結果より，フラボンがアミロイドイメージングプローブの基本骨格として機能することが示された．[21]

このアミロイドイメージングプローブとしてのフラボン誘導体の開発を契機に，さらにアミロイドイメージングプローブとして機能する分子骨格の探索研究を行った．新たな基本骨格として，フラボンに類似したスチリルクロモン，フラボンと同様のフラボノイドである，スチリルクロモン，[22] オーロン，[23] カルコン[24]を基本骨格に選択し，SPECT 用

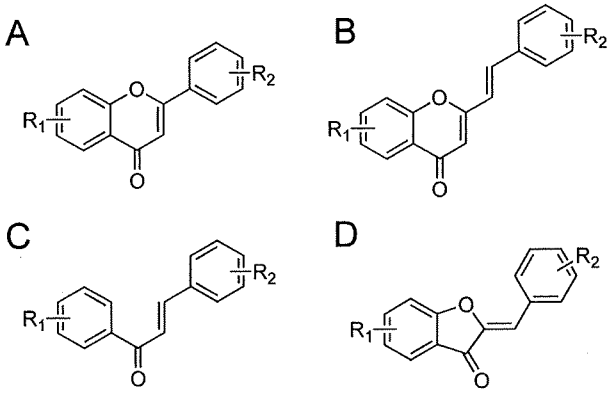

Fig. 8. Novel Pharmocophores for β-amyloid Imaging agents
(A): flavone, (B): styrylchromone, (C): chalcone, (D): aurone.

RI であるヨウ素と種々の置換基を導入した約 200 種類の化合物を合成した（Fig. 8）．老人斑アミロイドへの結合親和性の評価を行うために，アミロイド β ペプチドを用いたインビトロ結合実験を行い，18 個の化合物を選出し，さらに血液脳関門の透過性とクリアランスを検討するために，正常マウスにおける体内放射能分布実験を行い，IMPY のデータを評価基準に設けて，正常マウス脳への高い移行性と速やかなクリアランスを示した化合物 6 個を選出した．これらの化合物は，さらにアルツハイマー病の病態モデルマウス及びアルツハイマー病患者脳組織を用いる検討を行い，有望な結果を得始めている．

Figure 9 には，その中の 1 つである，オーロン骨格にヨウ素とエチレンオキシ基を導入した化合物を，アルツハイマー病モデルマウス（Tg2576）に投与 30 分後に屠殺後，凍結脳切片を作製し，蛍光染色と抗アミロイド β 抗体による免疫染色の結果を示す．その結果，モデルマウス脳切片上にオーロン誘導体の沈着に基づく多数の蛍光像が観察され，この蛍光像は，免疫染色の陽性部位と一致した．本検討結果は，オーロン誘導体が生体内アミロイド斑への結合性を示唆するものであり，さらに化合物の毒性評価等の臨床研究へ向けた準備を行っているところである．

さらに最近，核医学診断において最も汎用性に優れた RI である ^{99m}Tc を標識核種として用いたアミロイドイメージングプローブが報告され始めている．[25] これら化合物は，いずれもインビトロの検討において，アルツハイマー病患者及びアルツハイマー病モデルマウス脳内に沈着するアミロイド斑へ

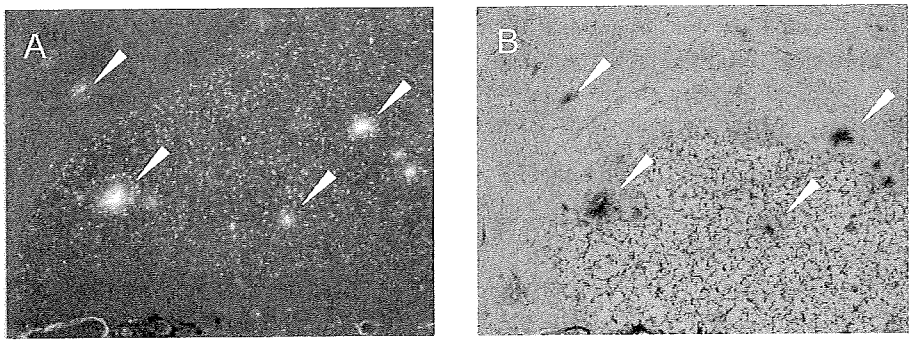

Fig. 9. Fluorescent Labeling of the Aurone Derivative after Injection into AD Model Mice (A), Immunohistologocal Staining with Anti β-Amyloid Antibodies in the Same Brain Section (B)

の結合性は保持されるが，脳移行性の低いことが問題となっており，この問題を改善した，さらに有用な ^{99m}Tc 標識プローブの開発が期待される．アルツハイマー病を含め，アミロイドタンパク質の凝集体が病因に関与する疾患がほかにも多く存在する（プリオン病，パーキンソン病，ハンチントン病等）．われわれが開発してきた一連のアミロイド結合性化合物は，これら疾患の診断用プローブになる可能性も考えられることから，さらに本研究を推進していきたいと考えている．

謝辞　本総説は，筆者が京都大学大学院薬学研究科及び長崎大学大学院医歯薬学総合研究科に在籍中に行った研究成果を中心に述べたものである．本研究に関する御指導を頂いた先生方，研究をともに行った大学院生，さらに共同研究をして下さった国内及び海外の研究者の多くの皆様に心から感謝を申し上げる．本稿に紹介した研究の一部は，新エネルギー・産業技術総合開発機構及び医薬基盤研究所の研究助成により実施されたものであり，記して謝意を表す．

REFERENCES

1) Buck A. K., Schirrmeister H., Hetzel M., Von Der Heide M., Halter G., Glatting G., Mattfeldt T., Liewald F., Reske S. N., Neumaier B., *Cancer Res.*, **62**(12), 3331–3334 (2002).
2) Shoup T. M., Olson J., Hoffman J. M., Votaw J., Eshima D., Eshima L., Camp V. M., Stabin M., Votaw D., Goodman M. M., *J. Nucl. Med.*, **40**(2), 331–338 (1999).
3) Hara T., Kosaka N., Shinoura N., Kondo T., *J. Nucl. Med.*, **38**(6), 842–847 (1997).
4) Chapman J. D., Baer K., Lee J., *Cancer Res.*, **43**(4), 1523–1528 (1983).
5) Fujibayashi Y., Taniuchi H., Yonekura Y., Ohtani H., Konishi J., Yokoyama A., *J. Nucl. Med.*, **38**(7), 1155–1160 (1997).
6) Blankenberg F. G., Katsikis P. D., Tait J. F., Davis R. E., Naumovski L., Ohtsuki K., Kopiwoda S., Abrams M. J., Strauss H. W., *J. Nucl. Med.*, **40**(1), 184–191 (1999).
7) Bakker W. H., Krenning E. P., Breeman W. A., Koper J. W., Kooij P. P., Reubi J. C., Klijn J. G., Visser T. J., Docter R., Lamberts S. W., *J. Nucl. Med.*, **31**(9), 1501–1509 (1990).
8) Sivolapenko G. B., Skarlos D., Pectasides D., Stathopoulou E., Milonakis A., Sirmalis G., Stuttle A., Courtenay-Luck N. S., Konstantinides K., Epenetos A. A., *Eur. J. Nucl. Med.*, **25**(10), 1383–1389 (1998).
9) Keenan A. M., Harbert J. C., Larson S. M., *J. Nucl. Med.*,**26**, 531–537 (1985).
10) Ono M., Arano Y., Mukai T., Saga T., Fujioka Y., Ogawa K., Kawashima H., Konishi J., Saji H., *Bioconjug. Chem.* **13**(3), 491–501 (2002).
11) Arano Y., Fujioka Y., Akizawa H., Ono M., Uehara T., Wakisaka K., Nakayama M., Sakahara H., Konishi J., Saji H., *Cancer Res.* Jan 1, **59**(1), 128–134 (1999).
12) Shoghi-Jadid K., Small G. W., Agdeppa E. D., Kepe V., Ercoli L. M., Siddarth P., Read S., Satyamurthy N., Petric A., Huang S. C., Barrio J. R., *Am. J. Geriatr. Psychiatry* **10**(1), 24–35 (2002).
13) Klunk W. E., Engler H., Nordberg A., Wang Y., Blomqvist G., Holt D. P., Bergström M., Savitcheva I., Huang G. F., Estrada S., Ausén B., Debnath M. L., Barletta J., Price J. C., Sandell J., Lopresti B. J., Wall A., Koivisto P., Antoni G., Mathis C. A., Långström B., *Ann. Neurol.*, **55**(3), 306–319 (2004).
14) Verhoeff N. P., Wilson A. A., Takeshita S., Trop L., Hussey D., Singh K., Kung H. F., Kung M. P., Houle S., *Am. J. Geriatr. Psychiatry*, **12**(6), 584–595 (2004).
15) Newberg A. B., Wintering N. A., Clark C. M., Plossl K., Skovronsky D., Seibyl J. P., Kung M. P., Kung H. F., *J. Nucl. Med.*, **47**, 78 (2006).
16) Kudo Y., Okamura N., Furumoto S., Tashiro M., Furukawa K., Maruyama M., Itoh M., Iwata R., Yanai K., Arai H., *J. Nucl. Med.*, **48**(4), 553–561 (2007).
17) Rowe C. C., Ackerman U., Browne W., Mulligan R., Pike K. L., O'Keefe G., Tochon-Danguy H., Chan G., Berlangieri S. U., Jones G., Dickinson-Rowe K. L., Kung H. P., Zhang W., Kung M. P., Skovronsky D., Dyrks T., Holl G., Krause S., Friebe M., Lehman L., Lindemann S., Dinkelborg L. M., Masters C. L., Villemagne V. L., *Lancet Neurol.*, **7**(2), 129–135 (2008).

18) Klunk W. E., Lopresti B. J., Ikonomovic M. D., Lefterov I. M., Koldamova R. P., Abrahamson E. E., Debnath M. L., Holt D. P., Huang G. F., Shao L., DeKosky S. T., Price J. C., Mathis C. A., *J. Neurosci.*, **25**(46), 10598–10606 (2005).
19) Maeda J., Ji B., Irie T., Tomiyama T., Maruyama M., Okauchi T., Staufenbiel M., Iwata N., Ono M., Saido T. C., Suzuki K., Mori H., Higuchi M., Suhara T., *J. Neurosci.*, **27**(41), 10957–10968 (2007).
20) Ono M., Kawashima H., Nonaka A., Kawai T., Haratake M., Mori H., Kung M. P., Kung H. F., Saji H., Nakayama M., *J. Med. Chem.*, **49**(9), 2725–2730 (2006).
21) Ono M., Yoshida N., Ishibashi K., Haratake M., Arano Y., Mori H., Nakayama M., *J. Med. Chem.*, **48**(23), 7253–7260 (2005).
22) Ono M., Maya Y., Haratake M., Nakayama M., *Bioorg. Med. Chem.*, **15**(1), 444–450 (2007).
23) Ono M., Haratake M., Mori H., Nakayama M., *Bioorg. Med. Chem.*, **15**(21), 6802–6809 (2007).
24) Ono M., Maya Y., Haratake M., Ito K., Mori H., Nakayama M., *Biochem. Biophys. Res. Commun.*, **361**(1), 116–121 (2007).
25) Chen X., Yu P., Zhang L., Liu B., *Bioorg. Med. Chem. Lett.*, **18**(4), 1442–1445 (2008).

Review

Development of Positron-Emission Tomography/Single-Photon Emission Computed Tomography Imaging Probes for *in Vivo* Detection of β-Amyloid Plaques in Alzheimer's Brains

Masahiro ONO

Department of Patho-Functional Bioanalyses, Graduate School of Pharmaceutical Sciences, Kyoto University; 46–29 Yoshida Shimoadachi-cho, Sakyo-ku, Kyoto 606–8501, Japan.

Received May 29, 2009

Currently, the development of radiotracers for *in vivo* imaging of β-amyloid plaques in Alzheimer's disease (AD) brains is an important, active area of molecular imaging. Postmortem brains of AD patients reveal neuropathologic features: the presence of β-amyloid plaques and neurofibrillary tangles, which contain β-amyloid peptides and highly phosphorylated tau proteins. Increases in the concentration of β-amyloid in the course of the disease lead to changes in AD brains. Thus, when used in combination with positron-emission tomography/single-photon emission computed tomography (PET/SPECT), β-amyloid imaging agents could serve as surrogate markers for the early diagnosis and neuropathogenetic studies of AD. Furthermore, quantitative evaluation of β-amyloid plaques in the brain could facilitate the evaluation of the efficacy of antiamyloid therapies that are currently being investigated. This paper reviews our research on the development of PET/SPECT imaging agents for *in vivo* detection of β-amyloid plaques in Alzheimer's brains.

Key words molecular imaging; Alzheimer's disease; β-amyloid; positron-emission tomography/single-photon emission computed tomography

Introduction

Alzheimer's disease (AD) is a neurodegenerative disease of the brain associated with irreversible cognitive decline, memory impairment, and behavioral changes. Postmortem brains of AD patients reveal neuropathologic features: the presence of senile plaques (SPs) and neurofibrillary tangles (NFTs), which contain β-amyloid (Aβ) peptides and highly phosphorylated tau proteins.[1,2] Although the precise mechanism of neuronal death in AD is still unknown, it is widely accepted that SPs and NFTs play a central role in its development. Currently, the only definitive confirmation of AD is by postmortem histopathologic examination of Aβ deposits in the brain. Therefore Aβ plaques in the brain may be useful as a biomarker for the differential diagnosis of AD, and the detection of individual Aβ plaques *in vivo* by positron-emission tomography (PET) or single-photon emission computed tomography (SPECT) should improve diagnosis and also accelerate discovery of effective therapeutic agents for AD.[3,4] A number of groups have worked to develop PET/SPECT imaging probes including [^{11}C]-2-4′-(methylaminophenyl)-6-hydroxybenzothiazole ([^{11}C]PIB),[5—8] [^{11}C]-4-*N*-methylamino-4′-hydroxystilbene ([^{11}C]SB-13),[9,10] [^{18}F]-4-(*N*-methylamino)-4′-(2-(2-(2-fluoroethoxy)ethoxy)ethoxy)-stilbene ([^{18}F]BAY94-9172),[11,12] [^{11}C]-2-(2-(2-dimethylaminothiazol-5-yl)ethenyl)-6-(2-(fluoro)ethoxy)benzoxazole ([^{11}C]BF-227),[13] [^{18}F]-2-(1-(2-(*N*-(2-fluoroethy)-*N*-methylamino)naphthalene-6-yl)ethylidene)malononitrile ([^{18}F]-FDDNP),[14—17] and [^{123}I]-6-iodo-2-(4′-dimethylamino)phenylimidazo[1,2-*a*]pyridine ([^{123}I]IMPY)[18—21] (Fig. 1). This paper reviews research on the development of PET/SPECT imaging agents for the *in vivo* detection of Aβ plaques in Alzheimer's brains.

PET Probes for Imaging of Aβ Plaques Derived from Stilbene and Benzofuran

As part of efforts to develop ^{11}C-labeled tracers for PET imaging of Aβ plaques in AD, we have evaluated a series of simple molecular probes. The minimum requirements for a

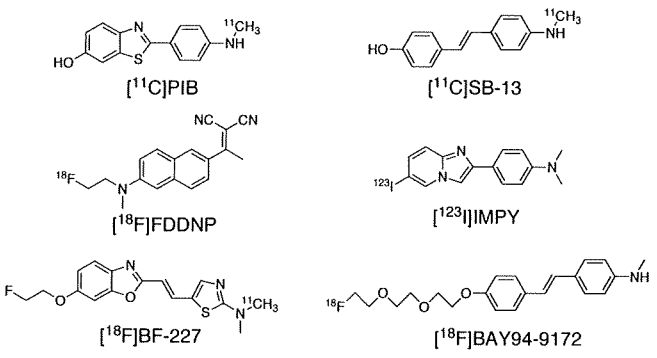

Fig. 1. Chemical Structure of Aβ Imaging Probes Clinically Tested

e-mail: ono@pharm.kyoto-u.ac.jp

Table 1. Inhibition Constants of Stilbene Derivatives on [^{125}I]TZDM Binding to Aβ(1—40) Aggregates

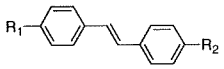

Compound	R_1	R_2	K_i (nM)[a]
1	NO_2	OCH_3	151±30
2	NH_2	OCH_3	36±5
3	$NHCH_3$	OCH_3	1.2±0.5
4	$NHCH_3$	OH	6.0±1.5
5	$N(CH_3)_2$	OCH_3	1.3±0.4
6	$N(CH_3)_2$	OH	2.2±0.6

a) Values are means±S.E. of three independent experiments.

successful Aβ-plaque-specific imaging agent include: small, neutral molecules; sufficient but moderate lipophilicity, good brain penetration; and low nonspecific binding in regions of the brain with no Aβ plaques. To meet the challenges of designing such molecules, we have investigated several series of core structures. One of them is a stilbene derivative, which is relatively simple and readily amenable to structural modification. A previous report suggested that the binding affinity to Aβ aggregates is associated with the essential substitution groups at the 4- and 4′-positions of the two phenol rings on the stilbene.[22] To balance the need to preserve the binding affinity and provide compounds with moderate lipophilicity, we have studied a series of simple stilbenes with 4-amino and 4′-hydroxy substitution groups (Table 1).

An *in vitro* binding assay using preformed Aβ(1—40) aggregates demonstrated that substituted stilbenes (**1**—**6**) competed with [^{125}I]TZDM, binding to Aβ(1—40) aggregates with excellent binding affinities. Among the stilbenes evaluated, it is evident that *N*-mono-methylated (**3**, **4**) or *N*,*N*-dimethylated (**5**, **6**) derivatives displayed higher binding affinities (K_i=1—6 nM). We are interested in selecting a compound with moderate lipophilicity and high binding affinity. To fulfill the need for opposing molecular properties, compound **4**, (K_i=6 nM) was selected as a compromise choice for ^{11}C labeling and further testing (Table 1).

In vitro autoradiography was performed by incubating [^{11}C]**4** with brain sections from control and double-mutation mice (TgCRDN8).[23,24] Using brain sections from these mice, Aβ plaque labeling by [^{11}C]**4** was tested. The labeled stilbene derivative, [^{11}C]**4**, showed an excellent binding to plaques in the mutant mouse brain sections, while only minimal labeling in control sections was observed (Fig. 2).

To examine the *in vivo* brain penetration, normal rats were injected with [^{11}C]**4**, and cortex and cerebellar regional brain tissue uptakes were determined at different time points

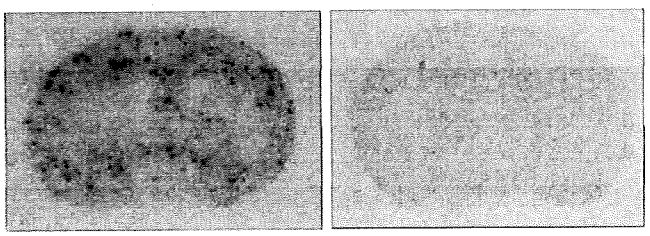

Fig. 2. *In Vitro* Autoradiographic Detection of Aβ Plaques with [^{11}C]**4** in TgCRND8 Mouse Brain Sections

Clear differences between histochemically characterized Tg Aβ(+) (left panel) and Tg Aβ(−) (right panel) brains are readily observable.

Table 2. Biodistribution of [^{11}C]**4** in Normal Rats after Intravenous Injection (% ID/g)[a]

Time (min)	Cortex	Cerebellum	Blood
2	1.15±0.08	1.15±0.08	0.61±0.07
15	0.74±0.05	0.71±0.01	0.39±0.01
30	0.42±0.03	0.41±0.02	0.29±0.01
60	0.30±0.03	0.31±0.01	0.24±0.02

a) Expressed as % injected dose per gram. Each value represents the mean±S.D. for 3 animals at each interval.

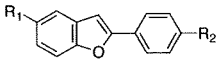

Fig. 3. Chemical Structure of Benzofuran Derivatives

Compounds here include the following: R_1=OCH_3, OH; R_2=NH_2, $NHCH_3$, $N(CH_3)_2$.

(Table 2). The initial brain uptake in the rat cortex was relatively high (1.15% dose/g, 2 min after intravenous (i.v.) injection), whereas the retention of [^{11}C]**4** in the brain was low (0.3% dose/g, 60 min after i.v. injection). A rapid washout rate suggests that the compound has low nonspecific binding in the brain, a highly desirable property for an Aβ imaging probe. Taken together, the data strongly suggest that the new ^{11}C-labeled stilbene compound, [^{11}C]**4**, may be a useful PET tracer for imaging Aβ plaques in the brain of patients with AD.[9]

In an attempt to develop more useful Aβ-specific imaging agents, we investigated a novel series of benzofuran derivatives, designed to be isosteric analogues of thioflavin-T (ThT) (Fig. 3).[25] We reported previously that iodinated benzofuran derivatives displayed excellent binding affinities for Aβ(1—40) aggregates (K_i=0.4—9.0 nM) and good brain penetration (>1.1% injected dose (ID) after i.v. injection in normal mice). However, the *in vivo* nonspecific binding of these probes, as reflected by their slow washout from the normal mouse brain, made them unsuitable for *in vivo* Aβ

Masahiro Ono is currently Associate Professor of Kyoto University. He was born in 1972 and graduated from Kyoto University in 1995. He received his Ph.D. in 2001 from Kyoto University under the supervision of Professor Hideo Saji. After that, he joined Nagasaki University under the supervision of Professor Morio Nakayama as an Assistant Professor in 2001. He worked as a postdoctoral fellow with Professor Hank F. Kung at the University of Pennsylvania for one and one-half years from 2001. He returned to Kyoto University and was promoted to Associate Professor in 2007. He received the Japanese Society of Nuclear Medicine Award for Young Scientists in 2008 and the Pharmaceutical Society of Japan Award for Young Scientists in 2009. His research interests are in the areas of radiopharmaceutical chemistry and molecular imaging.

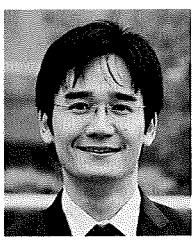

Masahiro Ono

plaque imaging.[26] These previous findings suggested that additional structural changes to these benzofurans may lead to the development of useful amyloid-specific imaging agents. Then, we designed and synthesized a new series of benzofuran derivatives (**7**—**12**) with low lipophilicity. An *in vitro* binding assay using AD brain homogenates demonstrated that substituted benzofuran derivatives competed with [^{125}I]IMPY binding to Aβ plaques with excellent binding affinities (Table 3). Comparing compounds **7**, **9**, and **11** with compounds **8**, **10**, and **12**, substitutions of the methoxy group at the 5-position with the hydroxy group resulted in only small changes in binding affinity. Compounds **9** and **10** with a monomethylaminophenyl moiety on the phenylbenzofuran molecule displayed slightly lower lipophilicity (higher binding affinity) as compared with compounds **7** and **8** with the aminophenyl moiety or compounds **11** and **12** with the dimethylaminophenyl moiety. However, all of the benzofuran derivatives evaluated maintained good binding affinity in the nanomolar range of K_i values. The results of the binding study strongly support our previous report that benzofuran derivatives have considerable tolerance for structural modification.[26] Some reports showed that preserving the binding affinity for Aβ plaques and providing compounds with moderate lipophilicity are prerequisites for successful Aβ imaging agents. Thus we selected compound **10**, with moderate lipophilicity and the highest binding affinity for Aβ plaques in AD brain homogenates, for ^{11}C-labeling and additional studies.

Next, compound **10** was investigated for its neuropathologic staining of SPs in human AD brain sections (Fig. 4). Compound **10** stained neuritic plaques, as well as cerebrovascular amyloid (Fig. 4, panels A and B). Since it is commonly assumed that neuritic plaques are formed even in very mild AD cases, and that the density of the neuritic plaques is associated with the severity of dementia and the number of neurons,[27,28] clear staining of Aβ plaques with compound **10** demonstrates that it is a promising compound and deserves further investigation as a potential tool for early diagnosis. Furthermore, compound **10** also displayed high binding affinity for NFTs in AD brain sections (Fig. 4C). A previous study reported that a marked increase in the amount of NFT accumulation in the hippocampus and entorhinal cortex was observed in the preclinical AD stage.[29] Because compound **10** intensely stained NFTs in human AD brain sections, it could detect increased NFT accumulation in the hippocampus and entorhinal cortex of the AD brain. These findings from the neuropathologic staining of human AD brain sections suggest that compound **10** can bind to Aβ plaques and NFTs with almost the same pattern of FDDNP[14] or X-34[30] previously reported, and quantitative evaluation of radiolabeled compound **10** in the brain may provide useful information on Aβ and tau pathology.

To predict the permeability of the blood–brain barrier (BBB), a 1-octanol/phosphate buffer (pH 7.4) partition coefficient of [^{11}C]**10** was examined. The log P value of [^{11}C]**10** was 2.36 at pH 7.4. Previous studies suggested that the optimal lipophilicity range for brain entry is observed for compounds with log P values between 1 and 3.[31] Below that range, passive diffusion through the BBB is poor; above that range, binding of any radiotracers to blood components (*e.g.*, red blood cells and albumin) is so great as to limit the amount available for brain entry. Since this ligand displayed moderate lipophilicity for BBB penetration, it was expected to show adequate brain uptake to detect Aβ plaques following systemic injection.

A biodistribution study in normal mice after intravenous injection showed that [^{11}C]**10** exhibited excellent brain uptake (4.8% ID/g of the brain at 2 min) and rapid washout (0.4 and 0.2% ID/g of the brain at 30 and 60 min, respectively), while the blood levels were relatively low at all time points measured (Table 4).

[^{11}C]PIB is currently the most widely utilized for detecting Aβ plaques in AD patients.[6,32,33] More recently, it has been reported that [^{11}C]**4** ([^{11}C]SB-13) also showed performance

Table 3. Inhibition Constants of Benzofuran Derivatives Using [^{125}I]IMPY as the Ligand in AD Brain Gray Matter Homogenates

Compound	K_i (nM)[a]
7	2.3±0.1
8	11.5±2.5
9	1.3±0.2
10	0.7±0.2
11	12.0±2.0
12	2.8±0.5

a) Values are means±S.E. of three independent experiments.

Table 4. Biodistribution of Radioactivity after Intravenous Injection of [^{11}C]**10** in Mice[a]

Time (min)	Brain	Blood
2	4.78 (1.10)	3.86 (0.36)
5	2.80 (0.63)	4.04 (1.14)
15	0.80 (0.31)	2.49 (0.67)
30	0.35 (0.08)	1.32 (0.41)
60	0.19 (0.04)	1.17 (0.14)

a) Expressed as % injected dose per gram. Each value represents the mean±S.D. for 4 animals at each interval.

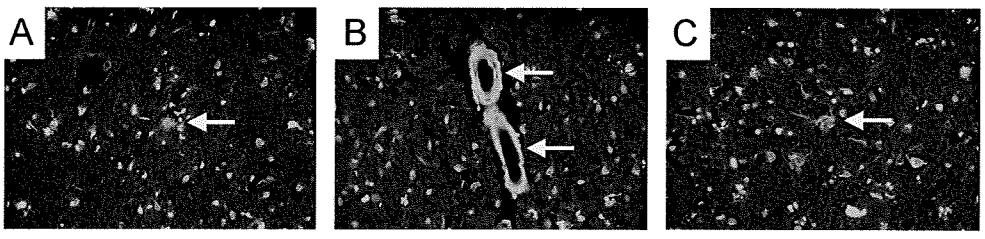

Fig. 4. Neuropathological Staining of Compound **10** on 5 μm AD Brain Sections from the Temporal Cortex

(A) Aβ plaques are clearly stained with compound **10** (×40 magnification). (B) Many cerebrovascular amyloids are intensely stained with compound **10** (×40 magnification). (C) Compound **10** also stained neurofibrillary tangles (NFTs) (×40 magnification).

similar to that of the more established tracer, [^{11}C]PIB.[10] Both tracers display appropriate properties for Aβ imaging agents: high binding affinity for Aβ plaques with K_i values of 4.3 and 6.0 nM for PIB and SB-13, respectively, in the *in vitro* binding assay; and high brain uptake and rapid clearance from the normal brain in animal studies. [^{11}C]PIB entered the brain rapidly (7.0% ID/g at 2 min after i.v. injection in mice) and cleared rapidly from normal mice brains (0.6% ID/g at 30 min after i.v. injection in mice). Since the ratio of 2—30-min mouse brain uptake after intravenous injection of [^{11}C]**10** was 0.07, which is comparable to that of [^{11}C]PIB, [^{11}C]**10** is also expected to have suitable *in vivo* pharmacokinetic properties for Aβ imaging in AD patients, similar to [^{11}C]PIB.

To confirm the *in vivo* labeling of Aβ plaques in the living mouse brain, we evaluated [^{11}C]**10** using a model mouse of AD, Tg2576 mice, which are specifically engineered to overproduce Aβ plaques in the brain. Autoradiographic images of Tg2576 mouse brain at 30 min after injection of [^{11}C]**10** showed high radioactivity accumulation in the cerebral cortex and hippocampus (Fig. 5A). In contrast, wild-type mouse brain displayed no marked accumulation of [^{11}C]**10** in the brain (Fig. 5A). Furthermore, we confirmed that the hot spots of [^{11}C]**10** in Tg2576 brains corresponded with those of *in vitro* thioflavin-S (ThS) staining in the same brain section (Fig. 5, panels B and C). The specific *in vivo* labeling of Aβ plaques demonstrates the feasibility of using it as an *in vivo* PET imaging agent for detecting Aβ plaques in the brains of AD patients.

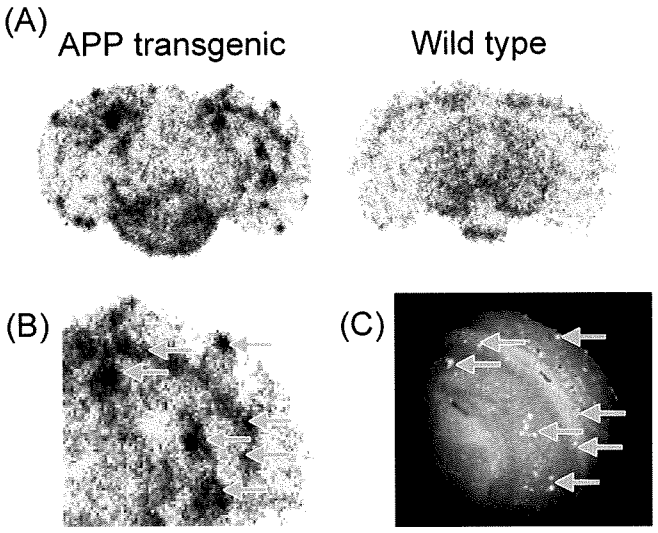

Fig. 5. *Ex Vivo* Plaque Labeling in Brain Sections from an APP Transgenic Mouse (A, B) and a Wild Type Mouse with [^{11}C]**10** (A)

Amyloid plaques were confirmed by *in vitro* staining of the same section with thioflavin-S (C). Arrows show amyloid plaques labeled by both [^{11}C]**10** and thioflavin-S.

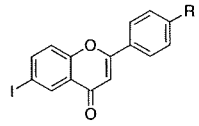

Fig. 6. Chemical Structure of Radioiodinated Flavone Derivatives

Compounds reported here include the following: R=NHMe (**13**), NMe_2 (**14**), OMe (**15**), OH (**16**).

SPECT Probes for Imaging of Aβ Plaques Derived from Flavonoid Compounds

Flavone-Based Aβ Imaging Probes It is well known that PET provides better functional information with higher resolution and greater sensitivity than SPECT. However, since SPECT imaging is more practical as a routine clinical diagnostic procedure, the development of Aβ imaging agents for SPECT has been highly anticipated. In an attempt to develop ^{123}I tracers for SPECT imaging, many radioiodinated probes based on various core structures have been studied. Among the radioiodinated ligands, [^{123}I]IMPY (Fig. 1) has been characterized as a potential SPECT imaging agent for Aβ plaques.[18,19] IMPY displayed selective Aβ plaque labeling in *ex vivo* autoradiography using double-transgenic mice (PSAPP) as a model of AD.[20] In addition, 2-(3′-iodo-4′-aminophenyl)-6-hydroxybenzothiazole (6-OH-BTA-O-3′-I) also showed desirable *in vitro* and *in vivo* properties.[34] However, clinically useful SPECT imaging agents have not been reported in humans.

Recently, the effects of polyhydroxyflavones on the formation, extension, and destabilization of Aβ aggregates have been studied *in vitro*.[35] These flavones dose dependently inhibited the formation of Aβ aggregates, as well as destabilizing preformed Aβ aggregates, indicating that they could interact directly with Aβ aggregates. The findings in that previous report prompted us to apply flavones as a novel core structure of Aβ imaging agents. Furthermore, some recent studies have shown that electron-donating groups such as methylamino, dimethylamino, methoxy, and hydroxy groups play a critical role in the binding affinity to Aβ aggregates.[5,9,19,22,26,36] With these considerations in mind, we designed four radioiodinated flavones with a radioiodine at the 6-position and an electron-donating group at the 4′-position (Fig. 6). Then we synthesized a series of flavone derivatives and evaluated their usefulness as *in vivo* SPECT Aβ imaging agents.[37]

Binding studies of [^{125}I]**14** to aggregates of Aβ(1—40) and Aβ(1—42) were carried out. Transformation of the saturation binding of [^{125}I]**14** to Scatchard plots gave linear plots, suggesting one binding site. [^{125}I]**14** showed excellent binding affinity for both Aβ(1—40) (K_d=12.4±2.3 nM) and Aβ(1—42) (K_d=17.4±5.7 nM) aggregates (Fig. 7). Binding affinities of nonradioactive flavone derivatives (compounds **13**, **14**, **15**, **16**) were evaluated in inhibition studies against [^{125}I]**14** binding on Aβ(1—40) and Aβ(1—42) aggregates. As shown in Table 5, all flavone derivatives competed well with [^{125}I]**14** binding on Aβ(1—40) and Aβ(1—42) aggregates. The K_i values estimated for **13**, **14**, **15**, and **16** were 23, 13, 29, and 73 nM for Aβ(1—40) aggregates and 30, 16, 38, and 77 nM for Aβ(1—42) aggregates, respectively. These K_i values suggest that the new series of flavones have high binding affinity for Aβ(1—40) and Aβ(1—42) aggregates in the following order: **14**>**13**>**15**>**16**. No marked difference between Aβ(1—40) and Aβ(1—42) aggregates was observed in the K_i values. It is especially noteworthy that compounds **13**, **14**, **15**, and **16** bound not only Aβ(1—40) aggregates but also Aβ(1—42) aggregates, as we aim to develop novel probes that can detect diffuse plaque deposits mainly composed of Aβ(1—42). More interestingly, when ThT and Congo Red (CR) were evaluated for their competition against [^{125}I]**14** binding on Aβ(1—40) and Aβ(1—42) aggregates,

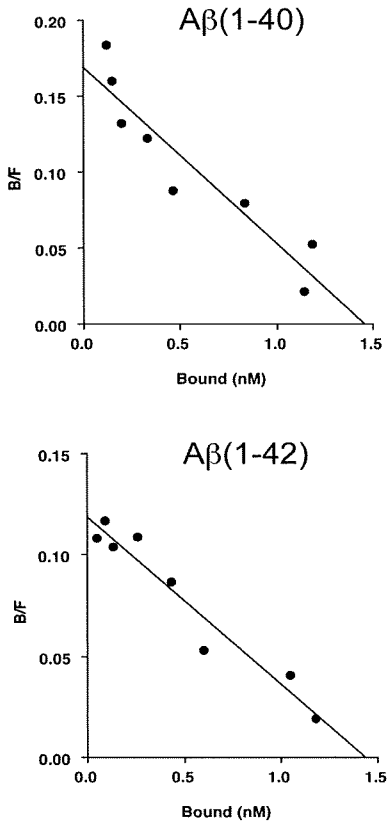

Fig. 7. Scatchard Plots of [^{125}I]**14** Binding to Aggregates of Aβ(1—40) and Aβ(1—42)

[^{125}I]**14** displayed one-site binding. High-affinity binding with K_d values in a nanomolar range was obtained (K_d=12.3 and 17.6 nM for Aβ(1—40) and Aβ(1—42) aggregates, respectively).

high K_i values (>1000 nM) were observed (Table 5), indicating poor binding competition. This finding suggests that these flavones may have a binding site on Aβ aggregates different from that of ThT and CR, although additional studies regarding the selectivity of binding affinity for Aβ aggregates are required.

Since the *in vitro* binding assays demonstrated the high binding affinity of the flavone derivatives for Aβ(1—40) and Aβ(1—42) aggregates, compounds **13**, **14**, **15**, and **16** were investigated for their neuropathologic staining of Aβ plaques and NFTs in human AD brain sections (Fig. 8). Compounds **13**, **14**, **15**, and **16** intensely stained Aβ plaques (Figs. 8A, E, I, M), neuritic plaques (Figs. 8B, F, J, N), and cerebrovascular amyloids (Figs. 8C, G, K, O) with nearly the same staining pattern. However, as seen in Figs. 8A, E, I, and M, these flavone compounds did not intensely stain the core region in so-called classic amyloid plaques, unlike the ThT and CR derivatives previously reported as Aβ imaging probes, indicating that flavone derivatives may have somewhat distinct binding characteristics for amyloid fibrils. The binding characteristics of the flavone derivatives for Aβ plaques in human AD

Table 5. Inhibition Constants (K_i, nM) of Compounds on Ligand Binding to Aggregates of Aβ(1—40) and Aβ(1—42)

Compound	Aβ(1—40)	Aβ(1—42)
13	22.6±3.4	30.0±3.4
14	13.2±0.2	15.6±2.4
15	29.0±3.2	38.3±8.1
16	72.5±8.2	77.2±9.2
ThT	>1000	>1000
CR	>1000	>1000

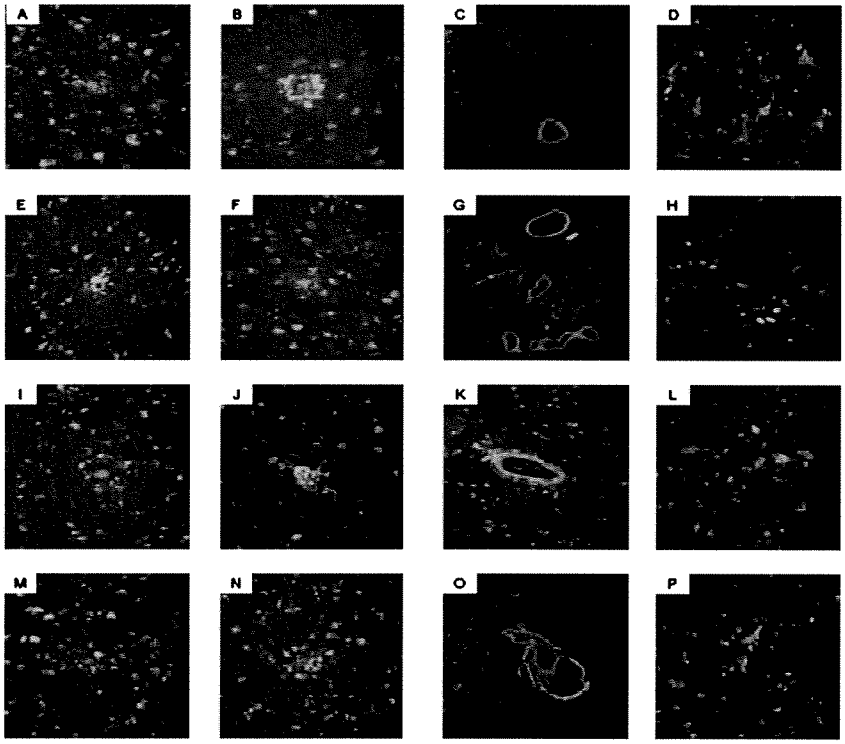

Fig. 8. Neuropathological Staining of Compounds **13** (A, E, I, M), **14** (B, F, J, N), **15** (C, G, K, O) and **16** (D, H, L, P) on 5 μm AD Brain Sections from the Temporal Cortex

(A) Aβ plaques (A—D) are clearly stained with compounds **13**, **14**, **15** and **16** (×40 magnification). Clear staining of neuritic plaques (E—H) and cerebrovascular amyloid (I—L) was also obtained. Many NFTs (M—P) are intensely stained with compounds **13**, **14**, **15** and **16** (×40 magnification).

sections may be relevant to the phenomenon observed in the *in vitro* binding assay: they may occupy a binding site on Aβ aggregates different from that of ThT and CR. Such a binding characteristic of the present flavone derivatives is thought to be related to the recent finding that a similar compound with a flavone backbone structure has binding affinity with amyloid fibrils and the APP sequence.[38] However, this issue regarding the binding property of flavone derivatives remains unresolved. These flavone derivatives appear to stain not only neuritic amyloid plaque but also diffuse amyloid plaque deposits, which are known to be mainly composed of Aβ(1—42)[39] and to be the initial pathologic change in AD.[40] Thus flavone derivatives with high binding affinity for Aβ(1—42)-positive diffuse plaques may be more useful for presymptomatic detection of AD pathology. Furthermore, compounds **13**, **14**, **15**, and **16** also showed high binding affinity for NFTs in AD brain sections (Figs. 8D, H, L, P). These findings suggest that the flavone derivatives **13**, **14**, **15**, and **16** can bind amyloid fibrils and NFTs without the backbone structure of ThT or CR and that quantitative evaluation of their cerebral localization may provide useful information on Aβ and tau pathology.

Four radioiodinated flavone ligands ([^{125}I]**13**, [^{125}I]**14**, [^{125}I]**15**, and [^{125}I]**16**) were evaluated for their *in vivo* biodistribution in normal mice. All four ligands examined in this study displayed optimal lipophilicity as reflected by their log P values of 1.94, 2.69, 2.41, and 1.92 for [^{125}I]**13**, [^{125}I]**14**, [^{125}I]**15**, and [^{125}I]**16**, respectively. As expected, these ligands displayed high brain uptakes ranging from 3.2 to 4.1% ID/g brain at 2 min postinjection, indicating a level sufficient for brain imaging probes (Table 6). In addition, they displayed good clearance from the normal brain with 1.2, 1.0, 0.17, and 0.08% ID/g at 60 min postinjection for [^{125}I]**13**, [^{125}I]**14**, [^{125}I]**15**, and [^{125}I]**16**, respectively (Table 6). These values were equal to 29%, 27%, 4.3%, and 2.4% of the initial brain uptake peak for [^{125}I]**13**, [^{125}I]**14**, [^{125}I]**15**, and [^{125}I]**16**, respectively. Radioiodinated amyloid imaging agents such as [^{125}I]TZDM,[36] [^{125}I]IBOX,[41] [^{125}I]*m*-I-stilbene,[22] and [^{125}I]benzofuran[26] reported previously showed high brain uptakes, but the washout rates from the normal brain were relatively slow. The slow washout rate from the brain leads to high background activity and prevents the visualization of Aβ plaques in the AD brain. The appropriate *in vivo* properties observed for radioiodinated flavones in the present study (higher brain uptake and faster washout from the normal brain) make them useful candidates for SPECT tracers for Aβ imaging.

Chalcone-Based Aβ Imaging Probes To search for more useful candidates in the development of *in vivo* Aβ imaging probes, we have designed a chemical modification of the flavone structure and selected the chalcone structure as a novel core for Aβ imaging probes (Fig. 9).[42,43] Chalcone is categorized as a member of the flavonoids containing flavone and has a chemical structure in which the ether linkage is removed from the flavone structure. Chalcone also contains a moiety structurally similar to curcumin (Fig. 9), which has been reported to have good brain permeability and favorable binding affinity to Aβ plaques after intravenous administration in Tg2576 transgenic mice.[44,45] Recently, radiolabeled curcumin derivatives have also been reported as Aβ imaging probes.[46] In addition to the structural characteristics of chalcone as the pharmacophore, some recent studies have shown that electron-donating groups such as amino, methylamino, dimethylamino, methoxy, or hydroxy groups play a critical role in the binding affinity to Aβ aggregates.[9,22,26,36] We therefore designed and synthesized novel chalcone derivatives and related chalcone-like compounds (**17**—**39**) (Fig. 10), and evaluated the effect of their structure–activity relationships on the binding affinity to Aβ aggregates and *in vivo* biodistribution using a compound with high binding affinity.

(*E*)-4-Dimethylamino-4′-[^{125}I]iodo-chalcone ([^{125}I]DMIC) was synthesized and used as the radioligand for competitive binding experiments (the K_d value of [^{125}I]DMIC is 4.2 nM).[42] Binding affinities of chalcone and chalcone-like compounds were evaluated in inhibition assays against [^{125}I]DMIC binding on Aβ(1—42) aggregates (Table 7). The K_i values suggested that the new series of chalcone and chal-

Table 6. Biodistribution of Radioactivity after Intravenous Injection of [^{125}I]**13**, [^{125}I]**14**, [^{125}I]**15**, and [^{125}I]**16** in Mice[a]

Tissue	Time after injection (min)			
	2	10	30	60
		[^{125}I]**13**		
Blood	1.89 (0.28)	1.39 (0.10)	1.34 (0.07)	1.50 (0.09)
Liver	16.28 (0.90)	25.28 (0.31)	18.61 (1.81)	15.14 (0.89)
Kidney	8.13 (1.28)	5.21 (0.44)	3.85 (0.33)	3.05 (0.25)
Intestine	3.10 (0.61)	7.91 (1.05)	12.84 (1.18)	21.48 (3.17)
Spleen	2.57 (1.54)	2.31 (0.01)	1.76 (0.23)	1.52 (0.29)
Heart	4.87 (0.66)	2.66 (0.12)	1.67 (0.14)	1.28 (0.12)
Stomach[b]	0.78 (0.02)	0.87 (0.22)	1.44 (0.69)	1.80 (0.84)
Brain	4.12 (0.15)	3.68 (0.18)	1.84 (0.12)	1.19 (0.04)
		[^{125}I]**14**		
Blood	1.87 (0.18)	1.07 (0.08)	1.20 (0.15)	1.15 (0.16)
Liver	15.41 (0.98)	21.85 (2.14)	15.71 (0.96)	12.40 (2.38)
Kidney	8.33 (1.47)	4.31 (0.28)	3.40 (0.31)	2.32 (0.45)
Intestine	2.24 (0.24)	6.56 (0.83)	12.97 (1.15)	18.64 (2.05)
Spleen	2.72 (0.20)	1.92 (0.33)	1.58 (0.31)	1.18 (0.17)
Heart	5.63 (0.80)	2.47 (0.14)	1.69 (0.06)	1.07 (0.17)
Stomach[b]	0.73 (0.17)	0.63 (0.16)	1.17 (0.40)	1.06 (0.27)
Brain	3.22 (0.15)	3.61 (0.60)	1.89 (0.21)	0.99 (0.10)
		[^{125}I]**15**		
Blood	1.87 (0.21)	1.19 (0.17)	0.40 (0.01)	0.23 (0.09)
Liver	8.96 (1.48)	9.01 (0.97)	3.75 (0.47)	1.88 (0.61)
Kidney	7.99 (1.08)	6.30 (1.02)	4.51 (1.59)	1.46 (1.12)
Intestine	3.52 (0.29)	14.39 (0.80)	22.51 (1.11)	30.05 (3.61)
Spleen	2.70 (0.08)	1.38 (0.37)	0.55 (0.30)	3.67 (5.89)
Heart	4.98 (0.41)	2.25 (0.40)	0.84 (0.14)	0.47 (0.22)
Stomach[b]	0.68 (0.06)	0.45 (0.18)	0.55 (0.33)	0.31 (0.07)
Brain	4.00 (0.18)	2.36 (0.33)	0.51 (0.07)	0.17 (0.05)
		[^{125}I]**16**		
Blood	2.77 (0.43)	1.58 (0.18)	0.66 (0.03)	0.20 (0.02)
Liver	9.77 (1.89)	8.24 (0.50)	6.80 (0.86)	4.78 (1.09)
Kidney	14.79 (2.59)	15.11 (2.00)	6.45 (0.84)	1.66 (0.62)
Intestine	3.12 (0.37)	11.26 (0.63)	22.01 (1.34)	27.28 (0.48)
Spleen	3.92 (1.18)	1.55 (0.15)	0.56 (0.13)	0.17 (0.06)
Heart	5.51 (0.71)	1.60 (0.18)	0.53 (0.04)	0.12 (0.02)
Stomach[b]	0.89 (0.09)	0.59 (0.16)	1.56 (0.50)	0.81 (0.36)
Brain	3.31 (0.32)	1.90 (0.07)	0.52 (0.03)	0.08 (0.02)

a) Expressed as % injected dose per gram. Each value represents the mean±S.D. for 3—5 animals at each interval. *b*) Expressed as % injected dose per organ.

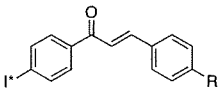

Fig. 9. Chemical Structure of Radioiodinated Chalcones